JAMES | Journal of Advances in Modeling Earth Systems

RESEARCH ARTICLE
10.1029/2019MS001799

Mean State Biases and Interannual Variability Affect Perceived Sensitivities of the Madden-Julian Oscillation to Air-Sea Coupling

N. P. Klingaman[1] and C. A. Demott[2]

[1]National Centre for Atmospheric Science and Department of Meteorology, University of Reading, Reading, UK, [2]Department of Atmospheric Science, Colorado State University, Fort Collins, CO, USA

Key Points:
- The response of the Madden-Julian oscillation (MJO) to coupling is sensitive to the representation of interannual variability
- Diagnosing intraseasonal coupled feedbacks to the MJO requires controling for interannual variability and mean state biases
- Air-sea coupling is not essential to simulate the MJO in the Super-Parameterized Community Atmospheric Model

Corresponding to:
N. P. Klingaman,
nicholas.klingaman@ncas.ac.uk

Citation:
Klingaman, N. P., & Demott, C. A. (2020). Mean-state biases and interannual variability affect perceived sensitivities of the Madden–Julian oscillation to air–sea coupling. *Journal of Advances in Modeling Earth Systems*, *12*, e2019MS001799. https://doi.org/10.1029/2019MS001799

Received 28 JUN 2019
Accepted 17 DEC 2019
Accepted article online 19 JAN 2020

Abstract Atmosphere-ocean feedbacks often improve the Madden-Julian oscillation (MJO) in climate models, but these improvements are balanced by mean state biases that can degrade the MJO through changing the basic state on which the MJO operates. The Super-Parameterized Community Atmospheric Model (SPCAM3) produces perhaps the best representation of the MJO among contemporary models, which improves further in a coupled configuration (SPCCSM3) despite considerable mean state biases in tropical sea surface temperatures and rainfall. We implement an atmosphere-ocean-mixed-layer configuration of SPCAM3 (SPCAM3-KPP) and use a flux-correction technique to isolate the effects of coupling and mean state biases on the MJO. When constrained to the observed ocean mean state, air-sea coupling does not substantially alter the MJO in SPCAM3, in contrast to previous studies. When constrained to the SPCCSM ocean mean state, SPCAM3-KPP fails to produce an MJO, in stark contrast to the strong MJO in SPCCSM3. Further KPP simulations demonstrate that the MJO in SPCCSM3 arises from an overly strong sensitivity to El Niño–Southern Oscillation events. Our results show that simulated interannual variability and coupled-model mean state biases affect the perceived response of the MJO to coupling. This is particularly concerning in the context of internal variability in coupled models, as many previous MJO sensitivity studies in coupled models used relatively short (20- to 50-year) simulations that undersample interannual-decadal variability. Diagnosing the effects of coupling on the MJO requires simulations that carefully control for mean state biases and interannual variability.

Plain Language Summary Many studies suggest that feedbacks between the atmosphere and ocean are essential for simulating the Madden-Julian oscillation, which controls weekly to monthly tropical rainfall. However, model experiments that diagnose the effect of these feedbacks are often not performed in a controlled manner, because introducing atmosphere-ocean feedbacks changes other aspects of the simulation, including the background climate and phenomena such as the El Niño–Southern Oscillation. These changes may affect the Madden-Julian oscillation as well, separately from direct atmosphere-ocean feedbacks, but these changes are often erroneously considered part of the sensitivity of the Madden-Julian oscillation to atmosphere-ocean feedbacks. We demonstrate that in one model that simulates the Madden-Julian oscillation well, the Super-Parameterized Community Atmospheric Model, intraseasonal atmosphere-ocean feedbacks alone do not substantially alter the Madden-Julian oscillation. Rather, the previously perceived improvement to the Madden-Julian oscillation from atmosphere-ocean feedbacks arises from a too strong response of the Madden-Julian oscillation to El Niño events. Future studies must carefully control for how introducing atmosphere-ocean feedbacks affects other aspects of the simulation, to better isolate the effect of those feedbacks on the Madden-Julian oscillation.

1. Introduction

The Madden-Julian oscillation (MJO; Madden & Julian, 1971) is a quasiperiodic (30- to 70-day), eastward propagating (≈5 m/s) mode of variability in the tropical climate system. Convective anomalies associated with the MJO are a key cause of rainfall variability throughout the tropics, including in the major monsoon regions (e.g., Lawrence & Webster, 2002; Lorenz & Hartmann, 2006; Wheeler et al., 2009). The associated circulation anomalies project strongly onto Zonal Wavenumber 1. At low levels, anomalous westerly winds are associated with the "active" (enhanced convection) phase of the MJO, while easterly anomalies are

associated with the "suppressed" (reduced convection) phase; the circulation is reversed at upper levels (e.g., Madden & Julian, 1972; Zhang, 2005). The passage of the MJO active phase enhances tropical cyclogenesis in all basins (e.g., Maloney & Hartmann, 2000; Camargo et al., 2008; Vitart, 2009). Teleconnections from MJO convective heating in the West Pacific extend into the midlatitudes, influencing the Pacific and Atlantic storm tracks (e.g., Cassou, 2008; Lin et al., 2009; Vitart & Molteni, 2010).

For more than 20 years, evaluations of climate-length simulations of general circulation models (GCMs) have concluded that GCMs struggle to represent the period, amplitude, and propagation speed of the MJO, as well as its effects on local and global circulation (e.g., Ahn et al., 2017; Hung et al., 2013; Jiang et al., 2015; Lin et al., 2008; Slingo et al., 1996; Zhang et al., 2006). Improvements to GCM representations of the MJO have come mainly from revising the subgrid-scale treatment of convection, particularly to increase the sensitivity of convection to free-tropospheric relative humidity (e.g., Hannah & Maloney, 2011; Hirons et al., 2013; Klingaman & Woolnough, 2014a). This reduces the erroneous tendency of convective parameterizations to produce excessive precipitation in anomalously dry regions, which leads to more intense MJO suppressed phases and stronger intraseasonal variability (ISV). These convective physics changes can degrade the simulated mean state, however, resulting in a tension between the simulated fidelity of ISV and the background climate (e.g., Benedict & Maloney, 2013; Johnson et al., 2015; Kim et al., 2011).

GCMs in which the conventional convective parameterization is disabled or replaced often produce an improved MJO. The parameterization is typically disabled only in sub-10-km resolution global or regional experiments (e.g., Holloway et al., 2013; Miyakawa et al., 2014). At coarser resolutions, so-called "superparameterized" (SP) GCMs replace inside each GCM grid box the parameterization with a two-dimensional cloud-resolving model that computes convective and radiative heating and moistening tendencies (Khairoutdinov et al., 2005). The SP configuration of the National Center for Atmospheric Research Community Atmospheric Model (SPCAM3) produces a coherent, eastward propagating MJO (Benedict & Randall, 2009), which improves with air-sea coupling in the Super Parameterized Community Climate System Model (SPCCSM3; Benedict & Randall, 2011; DeMott et al., 2014; Stan et al., 2010). SPCAM3 and SPCCSM3 were two of the highest-fidelity GCMs for the MJO in a comparison of 20-year climate simulations from more than two dozen models (Jiang et al., 2015). DeMott et al. (2014) demonstrated that SPCAM consistently produced a stronger and more realistic MJO than the standard (non-SP) CAM, even when both models were driven by the same prescribed, interannually varying sea surface temperatures (SSTs) from SPCCSM3. We analyze the same SPCCSM3 simulation in this manuscript.

Air-sea coupling in GCMs often also improves the MJO (DeMott et al., 2015, and references therein), although these improvements are usually secondary to those from modified convective physics (e.g., Klingaman & Woolnough, 2014b). In particular, well-resolved air-sea interactions—subdaily (typically 3 hr) air-sea exchanges and a fine (typically 1 m) oceanic vertical resolution—are required to capture the intraseasonal thermodynamic oceanic response to atmospheric forcing. Coarser spatial or temporal resolutions fail to simulate the peak diurnal SST warming and mixed-layer shoaling during the MJO suppressed phase, which rectifies onto intraseasonal scales (e.g., Bernie et al., 2005, 2008; Klingaman et al., 2011; Tseng et al., 2015). While the oceanic dynamical response to MJO forcing may be important for the development of subsequent MJO events that have no obvious atmospheric precursors (Webber et al., 2010, 2012), GCM experiments (e.g., Klingaman & Woolnough, 2014b; Tseng et al., 2015) and observational analysis (Halkides et al., 2015; Lau & Sui, 1997) show that most intraseasonal tropical SST variability can be recovered through thermodynamic air-sea interactions alone, particularly for regions more than $\pm 3°$ latitude from the equator. Recent comparisons of coupled (CGCM) and uncoupled (AGCM) configurations of four models, in which the CGCMs and AGCMs had identical SST climatologies, demonstrated coupling improved the MJO through enhanced mean meridional moisture gradients near the equator and strengthened convective moistening at high rain rates during the MJO active phase, helping to support equatorial convection and maintain column instability (DeMott et al., 2019). DeMott et al. (2019) included the same SPCCSM3 simulation that we analyze here.

In coupled GCMs with dynamical oceans, incorporating air-sea interactions inevitably leads to biases in the coupled mean state, such as cold SST biases in regions of excessive rainfall and associated strong turbulent fluxes into the atmosphere. These biases can degrade the simulated MJO by altering the background circulation and moisture fields to inhibit MJO propagation (e.g., Warm Pool easterlies rather than westerlies, cold

SST biases that limit convection and evaporation, reversals of mean zonal and meridional moisture gradients; Kim et al., 2017; Sperber et al., 2005; Zhang et al., 2006). Removing or damping these biases through flux corrections improves the MJO, demonstrating the strong control that the mean state exerts on subseasonal variability (Inness et al., 2003; Seo et al., 2007). Klingaman and Woolnough (2014b) found that cold tropical mean SST biases in the coupled Met Office Unified Model (MetUM) were associated with a poor MJO. The SST biases also influenced the perceived effect of air-sea interactions: Air-sea coupling appeared to have no impact on the MJO under the CGCM ocean mean state, but coupling improved the MJO when the ocean mean state biases were reduced through prescribed flux corrections.

It is not clear why in some GCMs (e.g., SPCCSM3) the apparent benefits of air-sea coupling for the MJO outweigh the degradations, while in other models (e.g., MetUM) the degradations outweigh the benefits. For SPCCSM3 in particular, no study has separated the effects of mean state errors and intraseasonal air-sea feedbacks to the MJO, to address whether the MJO in SPCCSM3 benefits from some aspect of the background state that is sensitive to coupling. For the intraseasonal MJO, the background state includes not only the time-mean climate but also coupled modes of interannual variability, including the El Niño–Southern Oscillation (ENSO) and the Indian Ocean Dipole (IOD), that influence tropical atmospheric and oceanic circulations. During El Niño, warm SSTs in the central Pacific encourage the MJO to propagate farther east (e.g., Tam & Lau, 2005; Woolnough et al., 2000); MJO events are also more frequent (e.g., Jones et al., 2004) and shorter-lived (Pohl & Matthews, 2007). Positive IOD events are linked to stronger MJO activity in the western Indian Ocean but limited propagation from the Indian Ocean to the Maritime Continent; negative IOD years show increased MJO activity in the eastern Indian Ocean (e.g., Wilson et al., 2013). Few studies have examined the effect on the MJO of CGCM biases in ENSO and IOD activity or of biases in teleconnections from these interannual modes to the MJO. Changes in these modes and their teleconnections represent another, potentially important, mechanism for air-sea coupling to influence the MJO. Further, previous studies of the SPCCSM3 MJO have identified the role of air-sea coupling MJO only under the biased SPCCSM3 mean state, by running "replay" experiments in which the SPCAM is forced by SPCCSM SSTs (DeMott et al., 2014). A more accurate assessment of the effects of coupling would compare coupled and atmosphere-only simulations under an SST mean state that is closer to observations, as recommended in DeMott et al. (2015).

We address the mechanisms by which coupling improves the MJO in SPCCSM3, using a set of experiments with a coupled atmosphere-ocean-mixed-layer configuration of SPCAM, in which the ocean mean state can be constrained to a target climatology. We employ this configuration to systematically isolate the effects of coupling on the MJO through (a) intraseasonal air-sea feedbacks, (b) mean state errors, and (c) ENSO activity. We describe this configuration, our experiments, and analysis techniques in section 2; identify the effects of coupling on the simulated MJO in section 3; discuss the implications of our results for future modeling studies of the role of coupling in the MJO in section 4; and summarize our key conclusions in section 5.

2. Models, Methods, and Data

2.1. Models

We analyze simulations with three model configurations based on SPCAM, Version 3 (SPCAM3; DeMott et al., 2007; Khairoutdinov et al., 2005, 2008): (a) an AGCM configuration (SPCAM3), in which SSTs and sea ice are prescribed as lower-boundary conditions; and two CGCM configurations in which SPCAM3 is coupled to (b) the Parallel Ocean Program (POP; Danbasoglu et al., 2006; Smith & Gent, 2004) three-dimensional ocean, which includes ocean dynamics (SPCCSM3; Stan et al., 2010) and (c) the Multi-Column configuration of the one-dimensional *K* Profile Parameterization boundary layer ocean model (MC-KPP; Large et al., 1994). We call (c) "SPCAM3-KPP" hereafter. In all simulations, we use T42L30 resolution: a triangular truncation at Wavenumber 42 in the horizontal (equivalent to ≈300 km at the equator) and 30 points in the vertical. The embedded cloud-resolving model in SPCAM3 is two-dimensional, with thirty-two 4-km-wide columns. In SPCCSM3, POP has a 10-m-thick top layer and exchanges SSTs and surface fluxes with SPCAM3 once per day. We focus the remainder of our discussion on SPCAM3-KPP, as the other configurations are documented in the studies above.

SPCAM3-KPP follows the design of the Global Ocean Mixed Layer coupled configuration of the Met Office Unified Model (MetUM-GOML; Hirons et al., 2015), in which one instance of KPP is placed under each atmospheric grid point. KPP uses a 1,000-m vertical domain, through which 100 points are unequally spaced, such that the vertical resolution is finest (≈1 m) near the surface, degrading to a constant 25 m through the

Table 1
For Each Experiment: the Name Used in the Text, the Model Used, the Length of the Simulation, the Oceanic Lower Boundary Condition (Coupling or Prescribed SST) and, for SPCAM3-KPP, the Target Ocean State to Which the Model Is Constrained

Name	Model	Length	Coupling or SST specification	Target ocean state
SPA-AMIP	SPCAM3	20 years	Reynolds et al. (2002)	N/A
SPC	SPCCSM3	20 years	Coupled to POP	N/A
SPK-OBS	SPCAM3-KPP	50 years	Coupled to KPP	1980–2009 mean from Smith and Murphey (2007)
SPA-KOBS	SPCAM3	50 years	31-day smoothed SPK-OBS	N/A
SPK-SPC	SPCAM3-KPP	50 years	Coupled to KPP	Climatology of SPC
SPA-KSPC	SPCAM3	50 years	31-day smoothed SPK-SPC	N/A
SPK-ENSO	SPCAM3-KPP	61 years	Coupled to KPP	3-year ENSO cycle from SPC
SPK-EN	SPCAM3-KPP	50 years	Coupled to KPP	SPC El Niño composite
SPK-LN	SPCAM3-KPP	50 years	Coupled to KPP	SPC La Niña composite
SPK-NN	SPCAM3-KPP	50 years	Coupled to KPP	SPC neutral ENSO composite

lowest ≈700 m of ocean. Because KPP lacks ocean dynamics, SPCAM3-KPP must be constrained to a target ocean climatology. We use this capability extensively, including constraining SPCAM3-KPP to a multiannual climatology of alternating ENSO states, described below. The constraints are applied via corrections to ocean temperature and salinity, made at all vertical grid points in each coupled column and at each time step. These corrections are computed from a simulation in which SPCAM3-KPP is relaxed toward the target climatology with a timescale of 15 days. In all cases, the length of this "tendency simulation" is 10 times the length of the target climatology (e.g., 10 years for an annual climatology and 30 years for a 3-year climatology) to obtain a robust estimate of the required corrections. We store the temperature and salinity relaxation tendencies from this simulation, and then we compute a daily climatology of corrections of the same length as the target ocean climatology; the climatology is also smoothed with a 31-day running mean, to remove high-frequency variability. This mean seasonal cycle of corrections is applied as a periodic (in time) forcing in a second, "free simulation" that can be integrated effectively infinitely. The free simulation has no relaxation, which avoids damping variability. Hirons et al. (2015) and Peatman and Klingaman (2018) demonstrated that multidecadal free simulations using this correction method had very small SST biases against the target ocean climatology. The corrections represent the effect of the mean ocean dynamics in SPCAM3-KPP and counteract coupled-model drift from errors in atmospheric surface fluxes.

Unlike MetUM-GOML, in which MetUM and MC-KPP exchange fields via a flux coupler, in SPCAM3-KPP the KPP ocean is implemented as a subroutine within SPCAM3. KPP uses the same time step as SPCAM3 (15 min), although this is purely for ease of coupling the models, not for computational stability; SPCAM3 and KPP exchange coupled fields each time step. Since SPCAM3-KPP lacks a sea ice model, SPCAM3 and KPP are not coupled at "ice-covered" grid points, which are points where the sea ice concentration is ≥0.3 for ≥30 days/year for ≥3 years in the 1980–2009 data set from the Atmospheric Model Intercomparison Project (AMIP) component of the Coupled model Intercomparison Project Phase 5 (Taylor et al., 2012), which is derived from Hurrell et al. (2008). Zero ice cover is assumed at all coupled grid points, including those in which the AMIP data set contains ice cover below the threshold above. There is no coupling over inland basins, such as the Great Lakes, or over the Red Sea. At uncoupled points, climatological sea ice from the AMIP data set and SSTs from the target ocean climatology are prescribed. A five–grid point blending between modeled and prescribed SSTs is imposed at all boundaries between coupled and uncoupled regions, with linearly decreasing weight given to the modeled SSTs further away from the coupled region.

2.2. Simulations

We refer to all simulations using first the letters "SPA" for SPCAM3 with prescribed SST, "SPC" for SPCCSM3, and "SPK" for a SPCAM3-KPP. For SPCAM3 and SPCAM3-KPP, we then use a code to identify the SST boundary condition (for SPCAM3) or the target ocean mean state (for SPCAM3-KPP); these are explained below. Table 1 summarizes the experiments.

We analyze data from 20-year SPCAM3 and SPCCSM3 simulations provided to the "Vertical structure and physical processes of the MJO" model evaluation project (Klingaman et al., 2015), specifically the 20-year

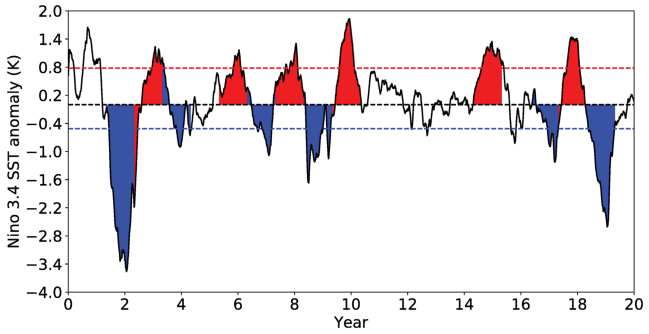

Figure 1. Time series of the Niño 3.4 SST index (K) from SPC. Shading shows the May–April periods selected for the (red) El Niño and (blue) La Niña composites; unshaded periods are used for the neutral composite. The red and blue dashed lines show the thresholds for El Niño and La Niña composites, respectively. Note that the thresholds are computed from, and applied to, the November–April mean index, while the May–April periods are shaded.

climate component (Jiang et al., 2015). SPCAM3 (hereafter "SPA-AMIP") was forced with prescribed weekly SSTs and sea ice concentrations from the National Oceanic and Atmospheric Administration (NOAA) Optimum Interpolation V2 data set (Reynolds et al., 2002). The SPCCSM3 simulation ("SPC") is the same as in Stan et al. (2010).

For SPCAM3-KPP, we perform a 50-year simulation ("SPK-OBS") with KPP constrained to the 1980–2009 climatology from the Met Office (UKMO) ocean analysis (Smith & Murphey, 2007). To isolate the effects of intraseasonal air-sea feedbacks on the MJO in SPK-OBS, we extract the daily SSTs from SPK-OBS, smooth them with a 31-day running mean to remove high-frequency variability and prescribe those SSTs in a 50-year SPCAM3 simulation ("SPA-KOBS"). High-frequency variability is removed following the analysis of Pegion and Kirtman (2008), DeMott et al. (2014) and others, summarized in DeMott et al. (2015), which found that high-frequency SSTs erroneously improved the simulated MJO due to an incorrect in-phase relationship between SSTs, surface fluxes, and rainfall. To isolate the effect of SPCCSM3 mean state SST errors on the MJO, we perform a 50-year SPCAM3-KPP simulation with MC-KPP constrained to the mean ocean state from SPC ("SPK-SPC"). To analyze the effects of intraseasonal air-sea feedbacks under the SPCCSM3 mean state, we extract the daily SSTs from SPK-SPC, smooth them with a 31-day running mean and prescribe them to SPCAM3 ("SPA-KSPC"). For each 50-year SPCAM3-KPP simulation, we first perform a 10-year simulation with relaxation, to compute the required climatological temperature and salinity corrections (section 2.1).

To isolate the role of the SPCCSM3 ENSO for the MJO (section 3.4), we partition SPC into three categories, based on terciles of the November–April (NDJFMA) mean Niño 3.4 SST index (SST anomalies averaged 5°S to 5°N, 180°–240°E; Figure 1). As there are only 19 November–April periods in the 20-year SPC simulation, we select the warmest six periods as "El Niño," the coldest six periods as "La Niña," and the remaining seven periods as "neutral." Mean seasonal cycles of ocean temperature and salinity are computed for each state, using May–April data to limit mixing ENSO phases. A 3-year composite ENSO cycle is formed by concatenating the 1-year climatologies for neutral, El Niño, and La Niña conditions, in that order. We perform a 30-year SPCAM3-KPP simulation with relaxation to this 3-year composite, to compute the mean 3-year cycle of temperature and salinity corrections necessary to maintain a target "mean state" of the repeating 3-year SPCCSM3 composite ENSO cycle. We then perform a 61-year SPCAM3-KPP simulation imposing those corrections ("SPK-ENSO") to obtain 20 complete 3-year cycles of May–April data. To test the sensitivity of the interannually varying ENSO signal on the MJO, we also perform a 50-year SPCAM3-KPP simulations constrained to a climatology of each phase of the SPC ENSO composite: El Niño (SPK-EN), La Niña (SPK-LN), and neutral (SPK-NN).

2.3. Methods

MJO propagation is evaluated through the standard technique of lag regressions of outgoing longwave radiation (OLR), which has first been filtered to an intraseasonal window (20–80 days, using a Lanczos filter with 181 weights) and latitude-averaged 10°S to 10°N. We use data for extended boreal winter, NDJFMA, because the MJO is most active during that period. We use regressions against a base point at 100°E, approximately the eastern boundary of the Indian Ocean, to focus on propagation from the Indian Ocean through the Maritime Continent to the West Pacific. This is a strict test of models, which often fail to propagate the MJO beyond the Indian Ocean (e.g., Jiang et al., 2015). We compare MJO propagation and strength in simulations and observations with three metrics. For propagation fidelity, we use the average pattern correlation of the observed and simulated regression maps at 100°E and 150°E, masking the longitudes within 15° of the base point. This tests MJO propagation through the Indian Ocean to the West Pacific (Jiang et al., 2015). Masking the region near the base point avoids high correlations in simulations that produce a standing oscillation (Wang et al., 2017; DeMott et al., 2019). For propagation speed, we use the average of the time between the maximum regressions at 70°E and 100°E and between 100°E and 130°E. For strength, we use the standard deviation of 20- to 80-day filtered OLR in the box 10°S to 10°N, 90–100°E. Metrics for all simulations and observations can be found in Table 2.

Table 2
For Each Observational and Model Data Set Analyzed in This Manuscript, Metrics of MJO Propagation Fidelity (Based on the Pattern Correlation of Hövmoller Diagrams With NOAA Observations; Unitless), MJO Intensity (Standard Deviation of 20- to 80-Day Band-Pass-Filtered OLR Anomalies in 10°S to 10°N, 90–100°E; W/m^2), and MJO Propagation Speed (Averaged 70–100°E and 100–130°E; ° Longitude per Day)

Data set	Pattern	Intensity (W/m^2)	Speed (°/day)
NOAA	1.00	14.03	4.37
SPC	0.82	15.02	4.72
SPK-OBS	0.81	18.90	5.86
SPA-KOBS	0.80	18.20	4.37
SPK-SPC	0.48	14.20	−1.00
SPA-KSPC	0.52	13.86	−0.06
NOAA (El Niño)	0.92	13.41	4.02
NOAA (neutral)	0.96	14.54	4.02
NOAA (La Niña)	0.87	13.88	4.17
SPC (El Niño)	0.82	15.72	4.17
SPC (neutral)	0.65	15.64	5.25
SPC (La Niña)	0.61	17.14	4.64
SPK-ENSO	0.78	16.17	5.25
SPK-ENSO (El Niño)	0.77	14.99	6.67
SPK-ENSO (neutral)	0.60	16.17	6.50
SPK-ENSO (La Niña)	0.61	15.8	4.36
SPK-EN	0.95	12.76	6.25
SPK-NN	0.66	15.09	3.82
SPK-LN	0.58	15.75	2.82

Note. See the text for further details on the methods. Note that some data sets are analyzed for only one ENSO phase, which is noted in parentheses after the data set name. The pattern correlation of NOAA is 1.0 by definition.

To diagnose the influence of time-varying SSTs on the MJO in a CGCM, we employ the diagnostic framework of DeMott et al. (2016). In that study, the authors used a moist static energy (MSE) approach to understand the effect of variable SSTs on intraseasonal tropical convection. Using European Centre for Medium-range Weather Forecasts Interim reanalysis data (ERA-Interim), the authors decomposed the vertically integrated MSE budget ($\langle m \rangle$) and its time rate of change ($\frac{\partial \langle m \rangle}{\partial t}$) to determine the contributions from the latent (LH) and sensible (SH) fluxes. Reynolds decomposition was employed to separate the thermodynamic (SST-driven) and dynamic (wind-driven) components of the fluxes. The contributions of ISV in SST were computed by recalculating LH and SH from 61-day smoothed SSTs, then projecting the full and smoothed fluxes onto $\langle m \rangle$ and $\frac{\partial \langle m \rangle}{\partial t}$; the difference between these projections is the effect of SST ISV. Including the ISV in SST led to increased equatorial moistening and reduced off-equatorial moistening, favoring equatorial convection that would project strongly onto Kelvin wave modes.

2.4. Data Sets

Apart from the SST, sea ice and ocean temperature and salinity data sets mentioned above, we employ satellite-derived OLR data from NOAA Cooperative Institute for Research in Environmental Sciences data set for 1979–2013, available daily on a 2.5 ° × 2.5° grid. We use the same ERA-Interim reanalysis data as DeMott et al. (2016) (1986–2013) to compute the "SST effect" on LH and SH. Observed SST data for 1979–2013 are taken from the NOAA OI data set discussed above (Reynolds et al., 2002).

3. Results

3.1. The MJO in SPC

We briefly discuss the MJO propagation and tropical mean state in SPC. MJO propagation in SPC is covered in greater detail in DeMott et al. (2014) and Jiang et al. (2015), but it is useful to review the basic features

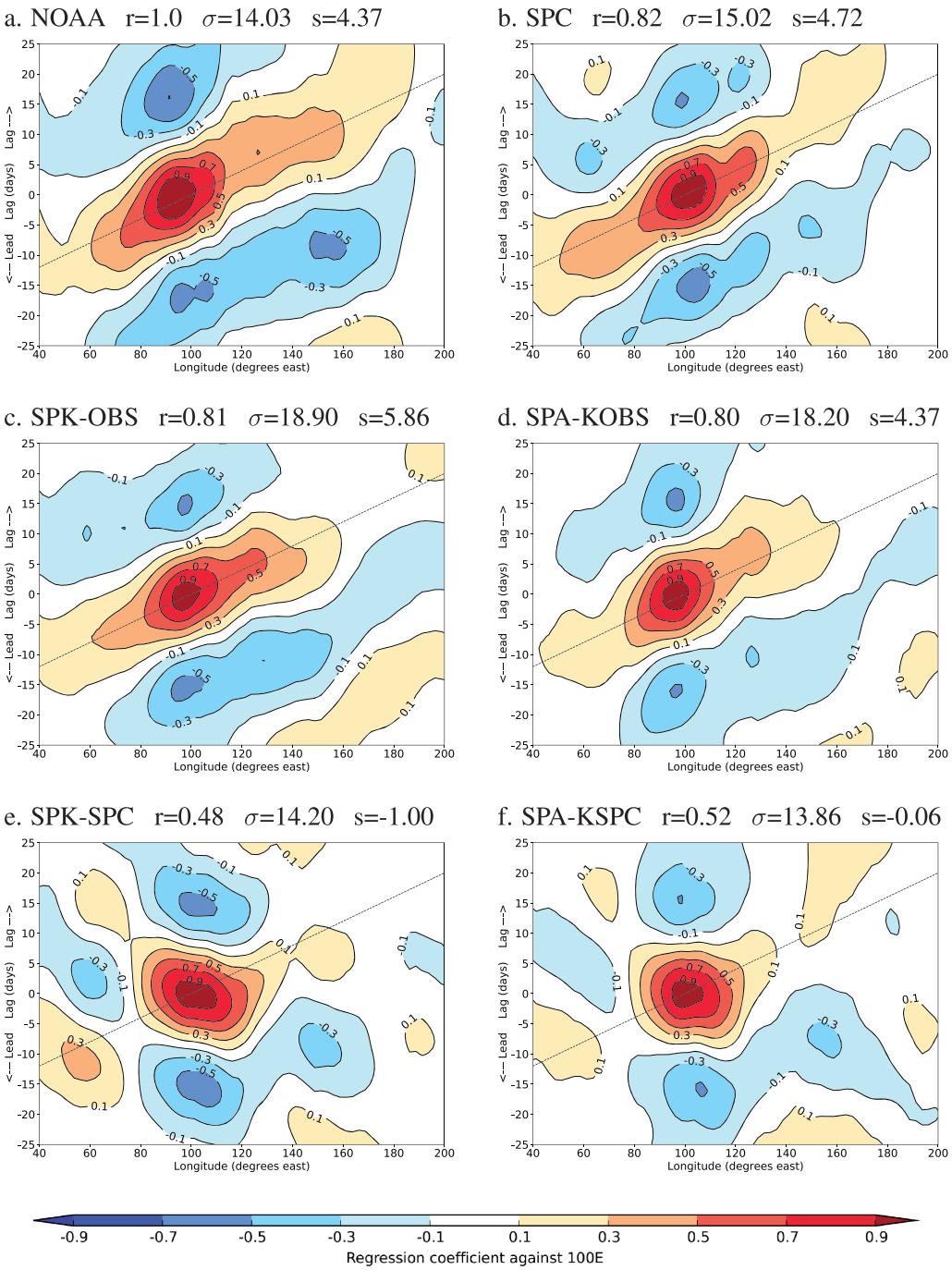

Figure 2. For NDJFMA data, lag regressions of 20- to 80-day filtered OLR (W/m^2, averaged 10°S to 10°N, against itself at a base point of 100°E for (a) NOAA satellite-derived observations, (b) SPC, (c) SPK-OBS, (d) SPA-KOBS, and (e) SPK-SPC. The dotted line shows an eastward propagation speed of 5 m/s. Units are W/m^2 per W/m^2 at the base point. The headings above each panel give metrics for propagation fidelity (r, pattern correlation against NOAA), strength (σ, W/m^2, standard deviation in 20- to 80-day OLR in 10°S to 10°N, 90–100°E) and propagation speed (°/day, averaged 70–100°E and 100–130°E). See the text for more details on the methods.

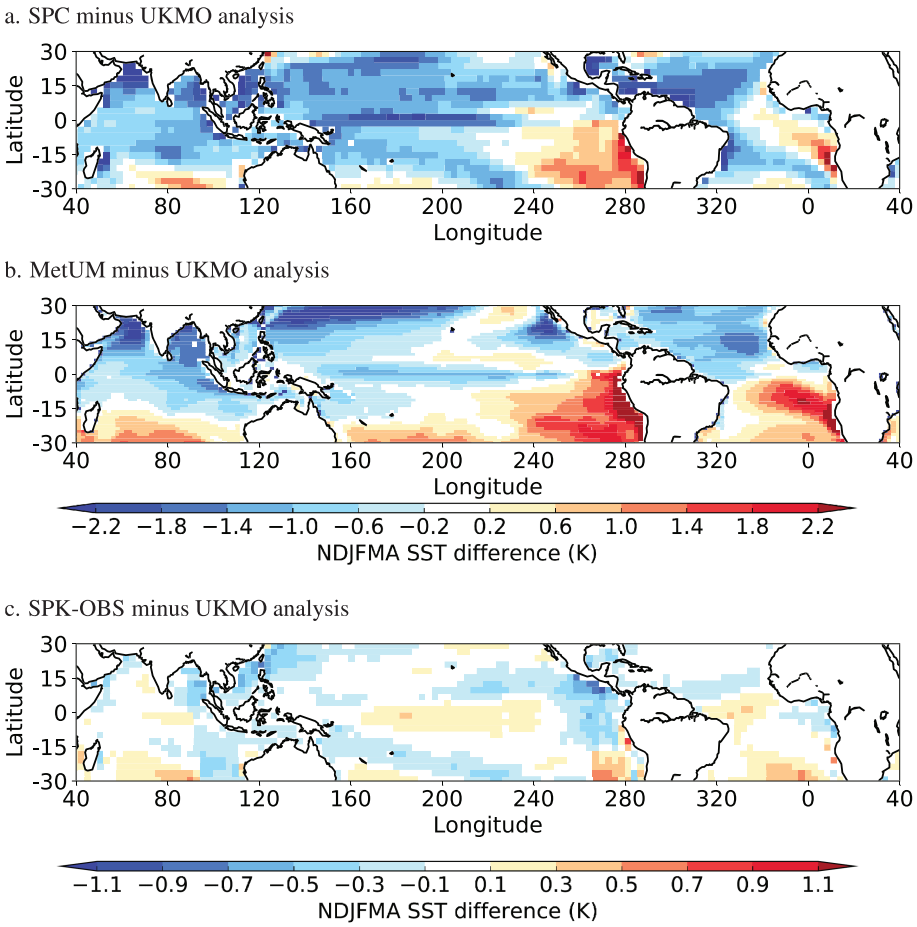

Figure 3. For NDJFMA data, SST biases (K) computed against the UKMO ocean analysis (1980–2009) for (a) SPC, (b) the MetUM "GA3-NEMO" simulation analyzed in Klingaman and Woolnough (2014b) and (c) SPK-OBS. Note that the contour interval in (c) is half of that in (a) and (b).

here as we compare our SPCAM3-KPP simulations to SPC in sections 3.2 and 3.3. SPC simulates a robust eastward propagating MJO from the Indian Ocean into the West Pacific (Figure 2b) that compares well with observations (Figure 2a). OLR regressions against 100°E are stronger over 100–130°E than in observations but weaker in the Indian Ocean and the West Pacific. This suggests that in SPC fewer MJO events propagate from the Indian Ocean to the Maritime Continent, but more events propagate across the Maritime Continent to the far western Pacific. DeMott et al. (2014) and DeMott et al. (2019) found that an SPCAM3 simulation with prescribed 31-day smoothed SSTs from SPC showed weaker MJO eastward propagation than SPC itself, which the authors concluded demonstrated that air-sea interactions play an important role in the strong eastward propagation in SPC.

SPC produces considerable cold SST biases throughout most of the tropics, both in NDJFMA (Figure 3a) and in the annual-mean (not shown). We compute biases against SSTs from the UKMO ocean analysis, as this is the climatology to which SPK-OBS is constrained and we wish to cleanly compare biases between SPC and SPK-OBS. SPC SST biases reach ≈-2.2 K west of the observed Pacific cold tongue region, the West Pacific warm pool, the Arabian Sea, and near the Maritime Continent. The pattern resembles an extended Pacific cold tongue. It weakens the zonal gradient of SST between the Indian Ocean and the Maritime Continent and enhances the zonal gradient between the Maritime Continent and central Pacific. The structure and magnitudes of the SST biases are remarkably similar to those from the MetUM "GA3-NEMO" simulation in Klingaman and Woolnough (2014b) (Figure 3b), which strongly damped the amplitude of the MetUM MJO. We return to the similarity between these mean states in section 4. SPC slightly underestimates ISV in equatorial SSTs (Figure 4c) relative to ERA-Interim (Figure 4a), with the greatest biases in the eastern equatorial Indian Ocean and northwest of Australia. ISV in precipitation is substantially overestimated,

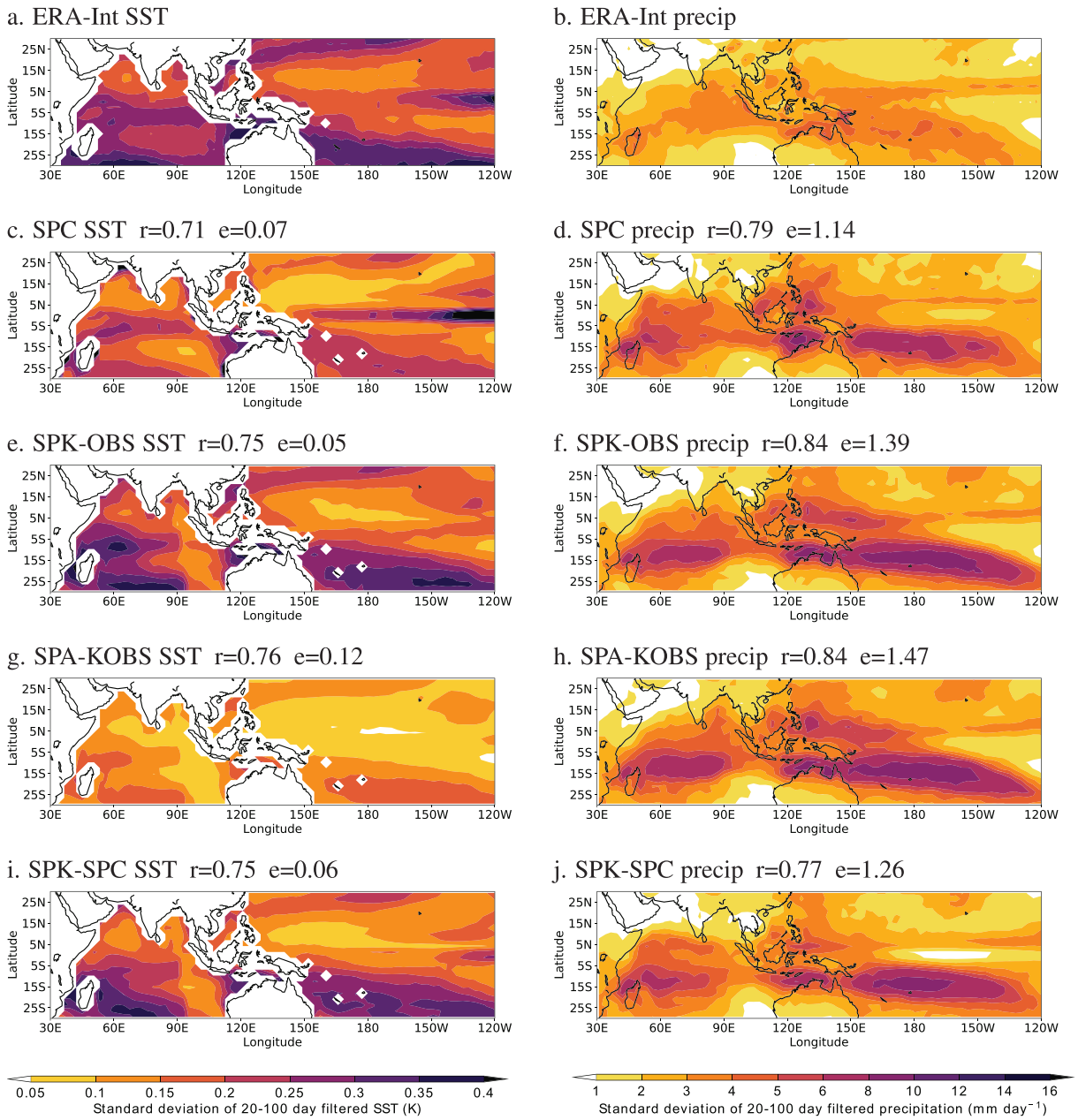

Figure 4. The standard deviation of 20- to 80-day filtered (left column) SSTs (K) and (right column) precipitation (mm/day), using data for NDJFMA only, from (a, b) ERA-Interim, (c, d) SPC, (e, f) SPK-OBS, (g, h) SPA-KOBS, and (i, j) SPK-SPC. For (c)–(j), the panel labels also show the pattern correlation (r) and root-mean-square error (RMSE, e) against ERA-Interim, using panel (a) for SST and panel (b) for precipitation, for the domain shown. For SST, data are masked where the land fraction in the grid box is smaller than 0.1; these points are not included in the correlation and RMSE metrics.

particularly in the western equatorial Indian Ocean, near the Maritime Continent, and in the South Pacific Convergence Zone (Figure 4d).

3.2. Air-Sea Coupling Under the Observed Ocean Mean State

First, we explore the tropical mean state and ISV in SPK-OBS, beginning with mean SST biases (Figure 3c) to establish that the temperature and salinity corrections effectively constrain SPCAM3-KPP to the target climatology, here from the UKMO ocean analysis. SST biases are smaller than ±0.5 K nearly everywhere and often smaller than ±0.3 K, particularly across the MJO domain; SPK-OBS biases are much smaller than those in SPC. For ISV, we compare the simulations to daily ERA-Interim SSTs, as the UKMO data are only monthly means. SPK-OBS (Figure 4e) accurately reproduces the spatial pattern and magnitude of SST ISV

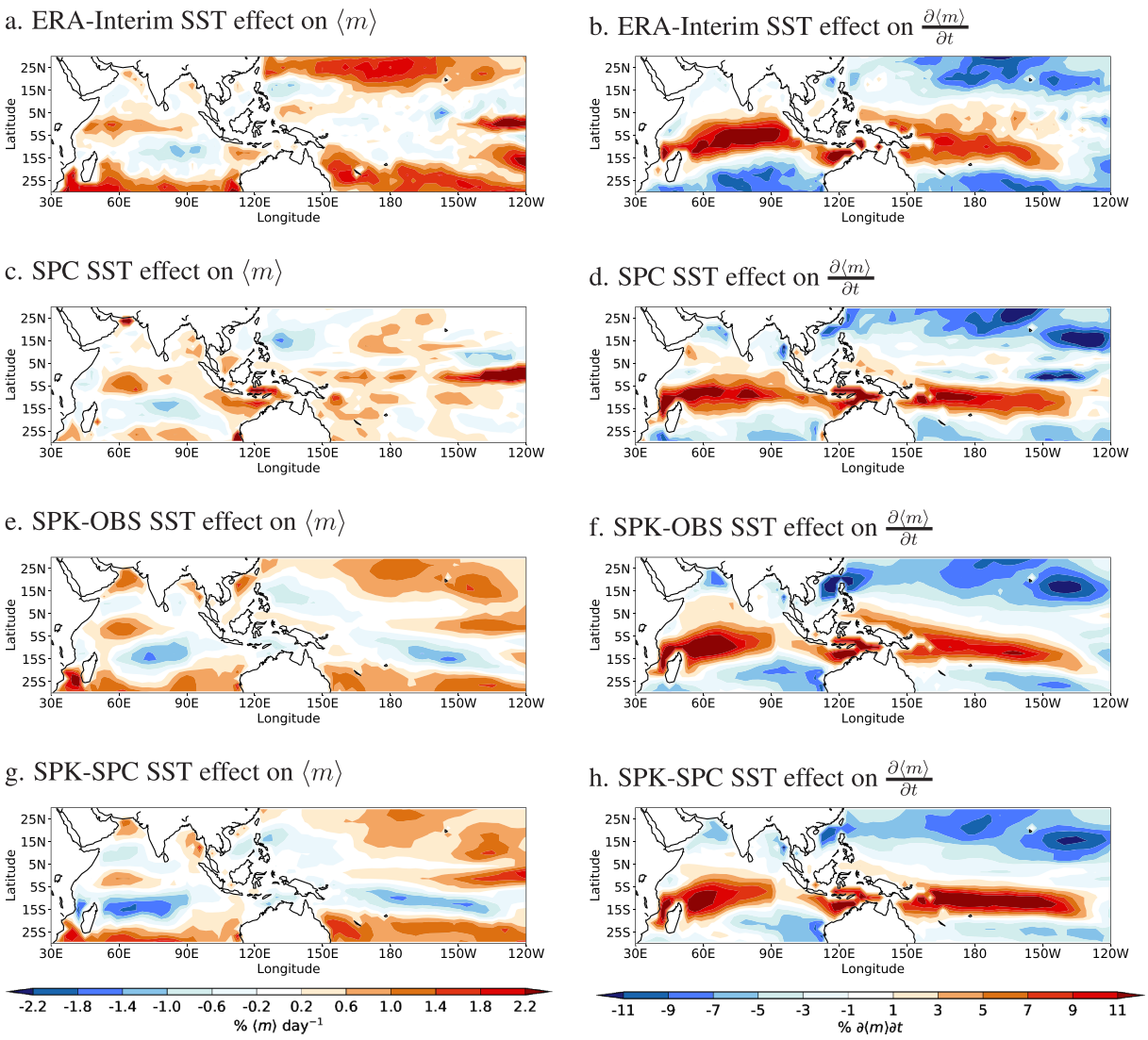

Figure 5. The "SST effect" through LH and SH on (left column) $\langle m \rangle$ and (right column) $\frac{\partial \langle m \rangle}{\partial t}$, computed as the difference in the projections onto either $\langle m \rangle$ or $\frac{\partial \langle m \rangle}{\partial t}$ of LH and SH computed with and without 61-day variability in SSTs. Data from (a, b) ERA-Interim, (c, d) SPC, (e, f) SPK-OBS, and (g,h) SPK-SPC. Units of all panels are percent per day of the quantity shown.

from ERA-Interim (Figure 4a), with higher ISV in the Seychelles thermocline ridge in the western Indian Ocean, in the shallow seas between the Maritime Continent and Australia and across the equatorial Indian Ocean. Tropical SST ISV is improved over SPC (Figure 4c) throughout the domain, particularly near the Maritime Continent, in the western equatorial Indian Ocean and in the subtropics. This supports many past studies that have shown that SST ISV improves in CGCMs with high vertical resolution (≈1 m) and subdaily coupling frequency (e.g., Bernie et al., 2008; Klingaman et al., 2011; Tseng et al., 2015) and that most SST ISV is thermodynamically driven, particularly away from the equator (e.g., Halkides et al., 2015; Lau & Sui, 1997). Relative to ERA-Interim (Figure 4b), SPK-OBS overestimates ISV in tropical precipitation, especially south of the equator in the Indian Ocean and in the South Pacific Convergence Zone (Figure 4d). Mean precipitation is also overestimated in these regions (not shown).

SPK-OBS captures coherent eastward propagation from the Indian Ocean to the West Pacific (Figure 2c), although the phase speed is faster than in NOAA (Figure 2a) and SPC (Figure 2b). On average, the SPK-OBS MJO does not propagate as far into the West Pacific as in NOAA, but the extent of propagation is similar to SPC. These results suggest that the smaller SST biases and larger ISV in tropical SSTs in SPK-OBS relative to SPC do not materially alter the MJO.

To diagnose the effect of intraseasonal (periods <61 days) SSTs on the MJO MSE budget, we compute the "SST effect" diagnostic for LH and SH (combined; section 2.3). In ERA-Interim, intraseasonal SSTs maintain $\langle m \rangle$ on the equator and discourage off-equatorial $\langle m \rangle$ (Figure 5a); intraseasonal SSTs also support $\frac{\partial \langle m \rangle}{\partial t}$ (equivalent to MJO propagation) in the eastern equatorial Indian Ocean and the West Pacific (Figure 5b; DeMott et al. (2016)). SPC displays a broadly similar pattern of SST effect for $\langle m \rangle$, with intraseasonal SSTs maintaining $\langle m \rangle$ in the equatorial Indian Ocean (Figure 5c). The effect of intraseasonal SSTs on $\frac{\partial \langle m \rangle}{\partial t}$ is generally weaker in the equatorial Indian Ocean in SPC than in ERA-Interim, although the effect is still positive (Figure 5d). Intraseasonal SSTs also influence the LH and SH contribution to $\langle m \rangle$ in SPK-OBS (Figure 5e), although the effect does not extend as far into the eastern Indian Ocean as in SPC. When combined with the relatively small contribution to $\frac{\partial \langle m \rangle}{\partial t}$ in the same region (Figure 5f), this may explain the somewhat weaker MJO propagation from the Indian Ocean to the Maritime Continent in SPK-OBS (Figure 2c). Indeed, SST ISV in SPK-OBS is small along the western coast of Sumatra, perhaps due to the lack in KPP of either wind-driven upwelling or warm-water advection by anomalous ocean currents in response to low-level anomalous easterly winds. SPK-OBS shows an increased subtropical SST effect relative to SPC, where the effect in SPC is too weak relative to ERA-Interim. This may be due to the increased SST ISV in SPK-OBS compared to SPC (Figure 4), which in turn may be associated with the increased oceanic vertical resolution or subdaily air-sea coupling in SPK-OBS. These diagnostics confirm that intraseasonal SSTs play a similar role in the MJO $\langle m \rangle$ budget in SPK-OBS as in SPC and that both simulations resemble the effect diagnosed from ERA-Interim.

The cleanest test of the effect of air-sea coupling in SPK-OBS is through comparison with the SPA-KOBS "replay" SPCAM3 simulation, in which the SPK-OBS 31-day smoothed SSTs are prescribed (e.g., DeMott et al., 2014; Klingaman & Woolnough, 2014b; DeMott et al., 2015). MJO propagation in SPA-KOBS is weaker than SPK-OBS, particularly from the Indian Ocean to the Maritime Continent, although the pattern correlation with NOAA is similar (Figure 2d). The MJO phase speed is slower in SPA-KOBS than SPK-OBS, bringing the speed closer to NOAA. Eastward propagation is still clearly evident, however, which confirms previous studies that found a robust MJO in SPCAM3 AMIP-type experiments (e.g., Khairoutdinov et al., 2008; DeMott et al., 2014). Smoothing the prescribed SSTs strongly damps ISV of SST in SPA-KOBS to less than half that in SPK-OBS (Figure 4g). This reduction is particularly severe in the eastern equatorial Indian Ocean, which may cause weak MJO propagation from the Indian Ocean to the Maritime Continent. Despite this reduction in SST ISV, SPA-KOBS produces slightly stronger precipitation ISV than SPK-OBS (Figure 4h), likely due to the tendency for AGCMs to generate excessive convection over warm intraseasonal SSTs relative to CGCMs, since the former lack negative local feedbacks through surface fluxes and SSTs (e.g., Pegion & Kirtman, 2008; DeMott et al., 2015; Hirons et al., 2018). These diagnostics suggest only modest effects of air-sea coupling on the MJO in SPCAM3 under a near-observed SST mean state, improving (increasing) MJO amplitude but degrading (quickening) propagation speed.

3.3. Air-Sea Coupling Under the SPC Ocean Mean State

Next, we consider the effect of changing from the UKMO analysis ocean mean state to the ocean mean state from SPC, by comparing SPK-SPC and SPK-OBS. It is important to highlight the differences between SPK-SPC and SPC: While the two have similar mean SSTs, SPC contains modes of coupled ocean-atmosphere variability (e.g., ENSO and IOD) that the MC-KPP ocean in SPK-SPC cannot represent; MC-KPP has finer vertical resolution than the POP ocean in SPC (1 and 10 m in the top layer, respectively) and a higher coupling frequency (15 min and 24 hr, respectively). The minimal differences between SPK-SPC and SPC in mean SST (Figure 6a) and precipitation and 850-hPa wind (Figure 6b) demonstrate the effectiveness of the SPCAM3-KPP correction technique.

Despite these small mean state differences, SPK-SPC lacks a propagating MJO (Figure 2e), in stark contrast to the strong and coherent MJO in SPC (Figure 2b) and SPK-OBS (Figure 2c). The cold tropical mean SST biases in SPC (Figure 3a) apparently suppress the MJO in SPK-SPC, in line with Klingaman and Woolnough (2014b) for MetUM, as well as with Inness et al. (2003), Sperber (2004), Zhang et al. (2006), and others. Using the SPC ocean mean state reduces SST ISV in SPK-SPC (Figure 4i) relative to SPK-OBS (Figure 4e), as expected for cooler mean SSTs. Precipitation ISV is also smaller in SPK-SPC (Figure 4j), with considerably lower variance in the equatorial Indian Ocean and the Maritime Continent. Yet the ISVs in precipitation and SST in SPK-SPC are broadly similar to those in SPC (Figures 4b and 4c), so it is unlikely that these reductions in variance can explain the degraded MJO in SPK-SPC. SPA-KSPC, an SPCAM3 simulation driven by 31-day smoothed SST from SPK-SPC, also fails to produce a propagating MJO (Figure 2f), which confirms that air-sea interactions are not responsible for the lack of an MJO in SPK-SPC.

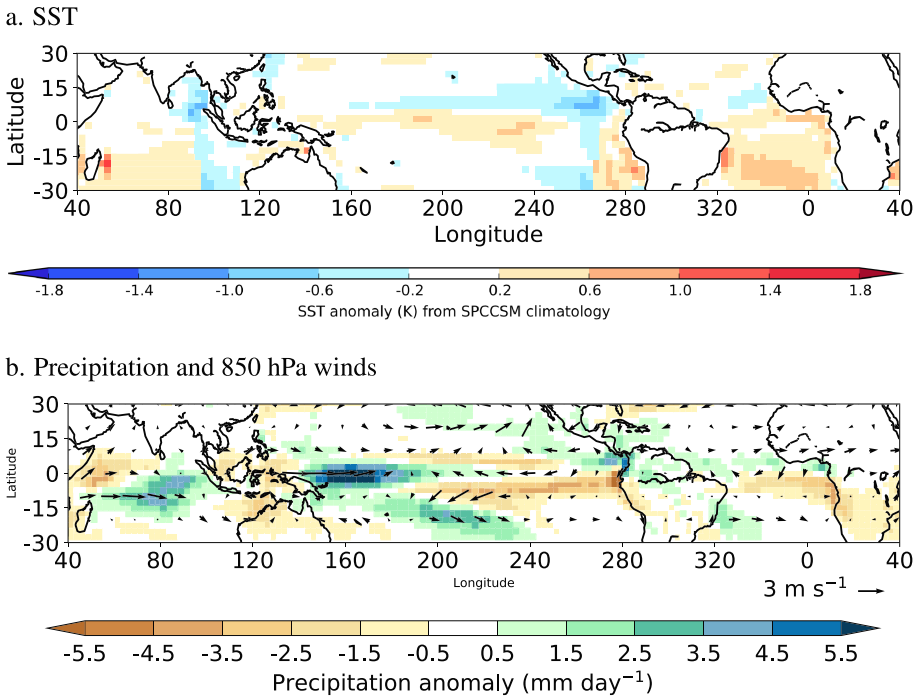

Figure 6. Using NDJFMA data, differences between SPK-SPC and SPC in mean (a) SSTs (K) and (b) precipitation (shading, mm/day) and 850-hPa winds (vectors, m/s).

Diagnostics of the "SST effect" on the MJO $\langle m \rangle$ budget are similar for SPK-SPC (Figures 5g and 5h) and SPC (Figures 5c and 5d). The contribution of intraseasonal SSTs through LH and SH to $\langle m \rangle$ remains positive in the equatorial Indian Ocean, as does the contribution to $\frac{\partial \langle m \rangle}{\partial t}$; the contribution to $\langle m \rangle$ is also negative in the off-equatorial regions, in agreement with ERA-Interim and SPC. Using the SPC mean state reduces the contribution to $\frac{\partial \langle m \rangle}{\partial t}$ in the equatorial Indian Ocean in SPK-SPC relative to SPK-OBS (Figure 5f), but as the contribution in SPK-SPC is similar to SPC it is unlikely to account for the degraded MJO. These diagnostics show that intraseasonal SSTs, and thus air-sea coupling, support MJO convection in SPK-SPC, which suggests intraseasonal SSTs alone are insufficient to produce an MJO in SPCAM3-KPP.

3.4. The Effect of ENSO

The results of section 3.3 imply that the MJO in SPC arises from some characteristic of SPCCSM3 that is missing in SPCAM3-KPP. Having shown that the mean state, ISV and effect of time-varying SSTs are similar in the two experiments, we investigate the effects of ENSO. While SPCAM3-KPP can produce weak, thermodynamically driven SST variability in the ENSO region (not shown), this variability is much smaller than in SPC (Figure 1); this variability in SPCAM3-KPP lacks the period and the phase locking to the seasonal cycle of the ENSO in observations or SPC.

First, we condition MJO propagation on ENSO phase in SPC and observations (Figure 7). We separate SPC by ENSO phase as in section 2.2. For observations (1979–2013), we apply the same method to separate observed NDJFMA Niño 3.4 SST anomalies into terciles. The influence of ENSO phase on MJO propagation in SPC is striking: MJO propagation beyond the Maritime Continent (130°E) occurs only in El Niño years (Figure 7a), in neutral (Figure 7c), and La Niña years (Figure 7e), MJO propagation is considerably weaker than in either the El Niño composite or the all-year composite (Figure 2b). Propagation is weaker not only from the Maritime Continent to the Pacific but also from the Indian Ocean to the Maritime Continent. In neutral years, the MJO suddenly jumps from Indian Ocean to the Maritime Continent; there is no smooth propagation. This suggests that there is a substantial rectification of the ENSO effect on the MJO onto the all-year composite: The MJO propagation in SPC appears strong only because the propagation is exceptionally strong in El Niño years.

Observations show a similar, but weaker effect of ENSO on MJO propagation: Propagation through the Maritime Continent is strong under El Niño (Figure 7b), remains evident in neutral years (Figure 7d), but

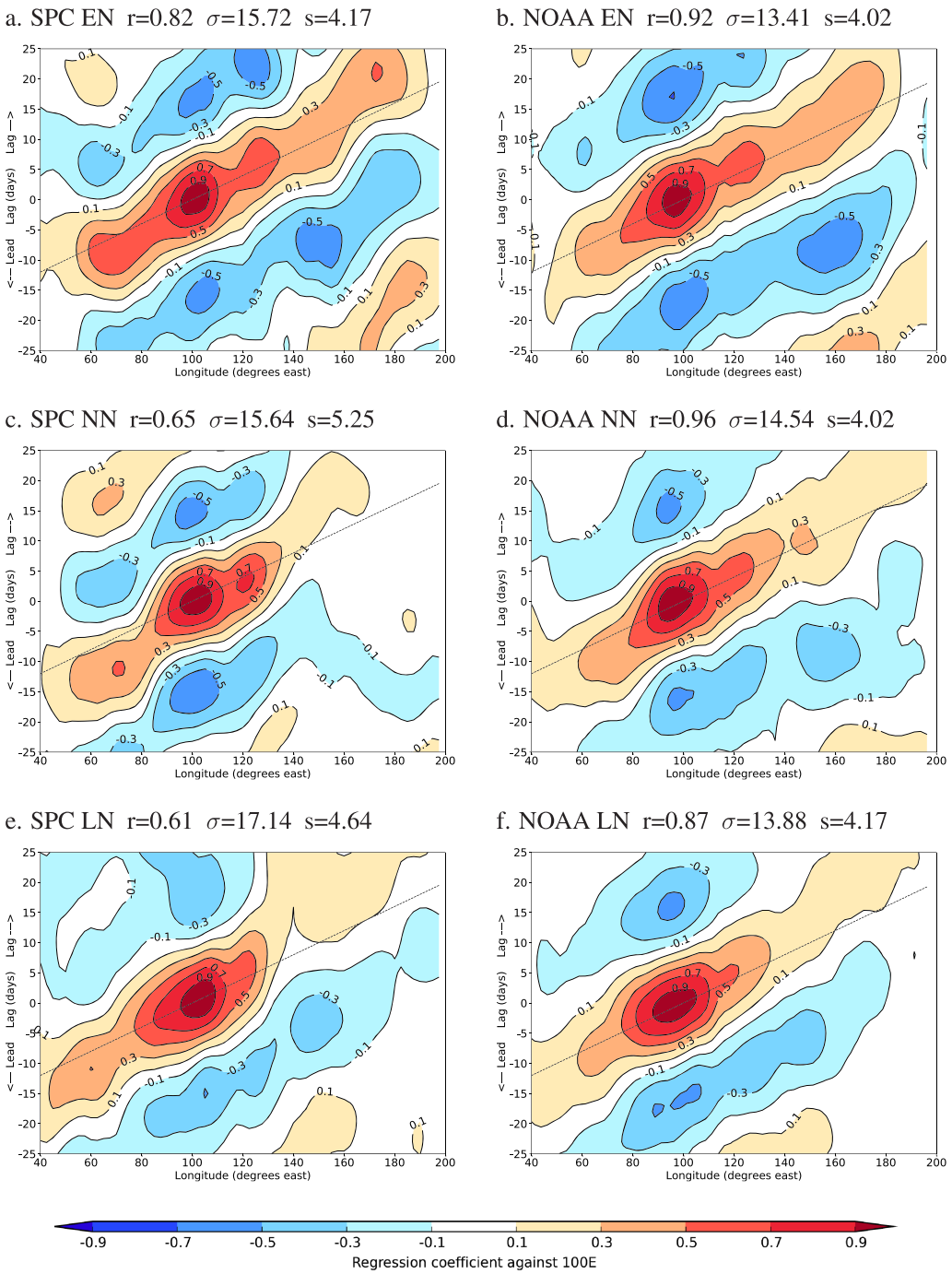

Figure 7. As in Figure 2 but conditioned on the phase of ENSO for (left column) SPC and (right column) NOAA satellite-derived OLR observations. Panels show (a, b) El Niño, (c, d) neutral ENSO, and (e, f) La Niña. Note that pattern correlations (r) are computed against the NOAA regression for all years (Figure 2 a).

weakens under La Niña (Figure 7f). Propagation from the Indian Ocean to the Maritime Continent is similar regardless of ENSO phase, unlike in SPC. Previous studies have shown similar results (e.g., Hendon et al., 1999; Gushchina & Dewitte, 2012; Tam & Lau, 2005; Woolnough et al., 2000). The major differences between SPC and observations are (a) a lack of propagation to the Pacific in neutral years in SPC and (b) weaker propagation in SPC through the Indian Ocean in neutral and La Niña years.

We hypothesize that the weakened propagation in neutral and La Niña years in SPC, relative to El Niño years, is associated with the cold tropical SST biases in SPC (Figure 3a). Composite SST anomalies in SPC by

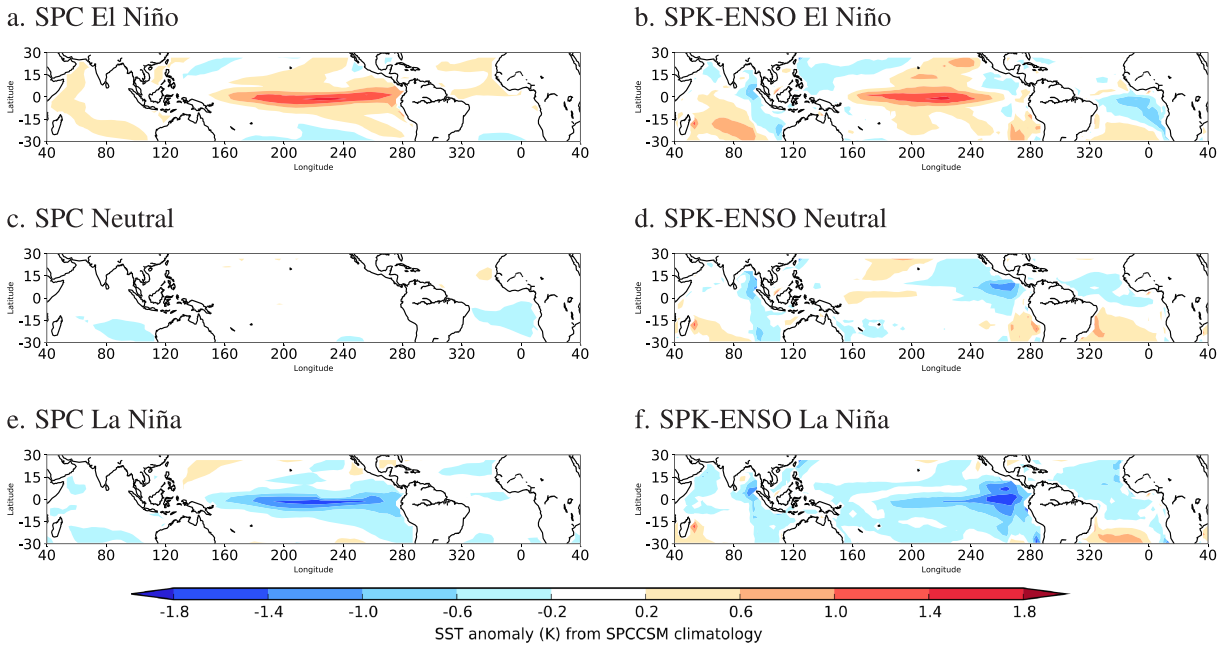

Figure 8. NDJFMA-mean SST anomalies (K) from the SPC climatology for (left column) SPC and (right column) SPK-ENSO, showing composites by ENSO phase: (a, b) El Niño, (c, d) neutral, and (e, f) La Niña. Note that SPK-ENSO anomalies are computed relative to the SPC climatology, to provide a clean comparison with the SPC anomalies.

ENSO phase show that the SPC El Niño SST anomaly (Figure 8a) is similar in structure and magnitude to the equatorial Pacific mean cold bias. Thus, El Niño in SPC effectively reduces the model's mean state error, which may allow the MJO to propagate further into the Pacific by altering the zonal gradient of SST across the Warm Pool. Neutral years have nearly zero SST anomaly (Figure 8c) and so retain the mean state bias, while La Niña years resemble an intensified mean state bias (Figure 8e).

To test the hypothesis that stronger propagation in El Niño years causes the improved MJO propagation in SPC, we assess MJO propagation in SPK-ENSO. In SPK-ENSO, MC-KPP is forced to reproduce the composite SPC 3-year ENSO cycle, which progresses neutral El Niño-La Niña (section 2.2). An advantage of SPCAM3-KPP is that this 3-year cycle can be reproduced effectively indefinitely, giving a large sample size of 20 El Niño periods (NDJFMA), 20 neutral periods, and 20 La Niña periods (Figure 9), determined by applying the same tercile-based classification as for SPC. SPK-ENSO reproduces the target climatology well, although the La Niña events are slightly weaker than the target event. As a result, the average SPK-ENSO El Niño event is stronger than the La Niña event. SPK-ENSO successfully reproduces the ENSO composite SST anomalies from SPC (Figures 8b, 8d, and 8f). The correction technique is less successful at constraining East Pacific SST, likely due to the substantial role for upwelling there, which cannot be captured by MC-KPP.

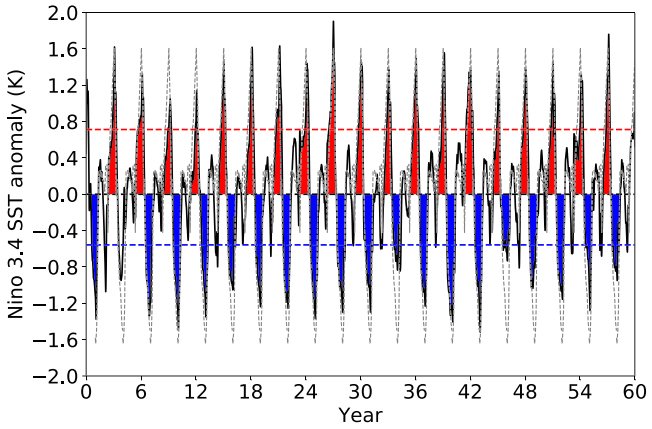

Figure 9. As in Figure 1 but for the SPK-ENSO simulation. The gray dashed line shows the Niño 3.4 index for the 3-year repeating target climatology derived from SPC.

Prescribing the 3-year composite ENSO cycle in SPK-ENSO also recovers the ENSO-driven anomalies in precipitation and 850-hPa winds in SPC (Figure 10). El Niño is associated with increased precipitation and westerly anomalies over the equatorial Pacific, while reduced precipitation and easterly anomalies prevail across the Maritime Continent and eastern Indian Ocean (Figures 10a and 10b). La Niña shows roughly the opposite pattern (Figures 10e and 10f). SPK-ENSO produces lower precipitation and slight easterly anomalies over the Maritime Continent relative to SPC in all ENSO phases, a factor which may be important for MJO propagation and to which we will return in section 4. This difference is most

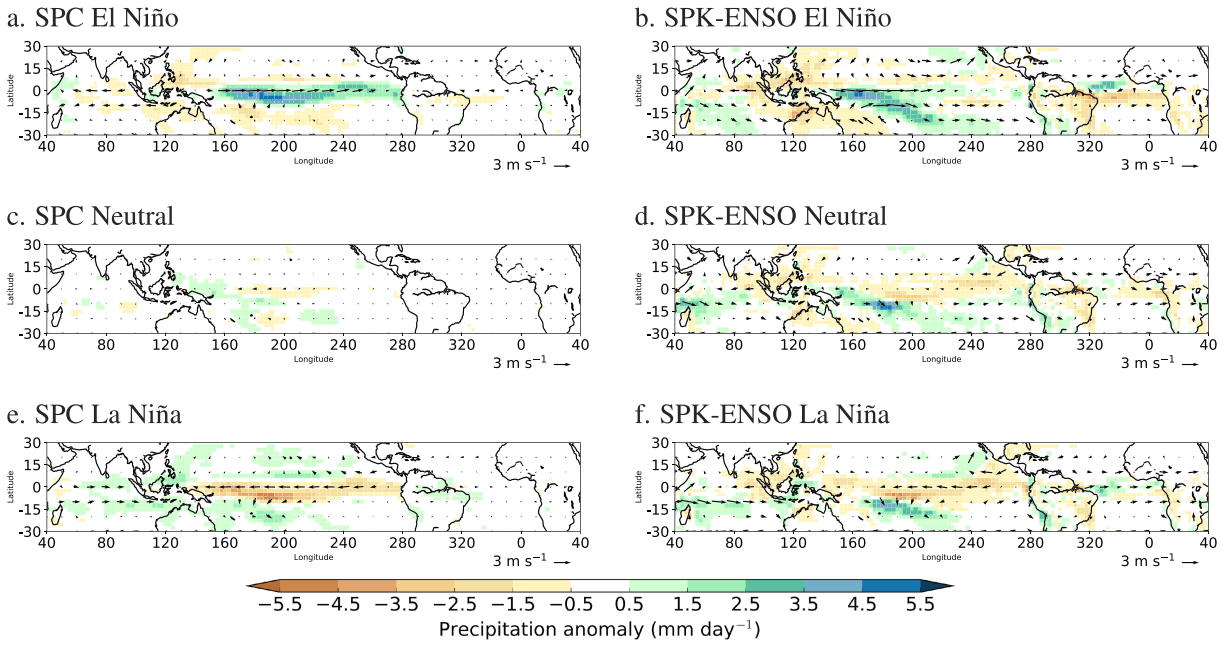

Figure 10. As in Figure 8 but for composites by ENSO phase of (shading) precipitation (mm/day) and (vectors) 850-hPa wind (m/s). Note that as in Figure 8, the SPK-ENSO anomalies are computed relative to the SPC climatology.

apparent in SPK-ENSO neutral composite (Figure 10d); it may be related to the cold SST bias west of the Maritime Continent in SPK-ENSO, relative to SPC (Figure 8d). We emphasize that while the MC-KPP corrections produce oceanic and atmospheric mean states that are very similar to the target climatology, small (but potentially important) differences remain.

The 3-year ENSO cycle in SPK-ENSO reproduces most of the MJO propagation behavior from SPC (Figures 11a and 11b). Overall propagation in SPK-ENSO is considerably improved over SPK-SPC (Figure 2e). As the only difference between these simulations is the composite ENSO cycle from SPC, ENSO variability is clearly essential to MJO propagation in SPC. As in SPC, when MJO propagation in SPK-ENSO is composited by ENSO phase, propagation through the Maritime Continent is strong only under El Niño (Figure 11c) with weaker or absent propagation in neutral and La Niña years. For any ENSO phase, or for all years, propagation in SPK-ENSO is somewhat weaker than for the same conditions in SPC. We hypothesize that this is due to the slightly colder SSTs in the eastern Indian Ocean in SPK-ENSO, alongside reduced precipitation and anomalous easterly lower-tropospheric winds near the Maritime Continent, or to associated differences in column water vapor during ENSO phases (Demott et al., 2018). For an active MJO in the Indian Ocean, such anomalies are consistent with reduced horizontal moisture advection from the east, a factor several studies have concluded is key for robust eastward MJO propagation in models (e.g., DeMott et al., 2014; Kim et al., 2017). While the strong MJO in El Niño years may support the El Niño event itself in SPC (e.g., through westerly wind bursts and oceanic Kelvin waves), it is unlikely that the SPC MJO triggers El Niño events, as the MJO is weak in non-El Niño conditions. Further, this mechanism cannot operate in SPK-ENSO, as MC-KPP lacks ocean dynamics.

While SPK-ENSO reproduces most of the behavior of SPC in each ENSO phase, as well as in all years, none of the ENSO-phase composites in SPK or SPC resemble the standing oscillation in SPK-SPC (Figure 2 e). Even in La Niña years, when ENSO increases the SPC mean state biases in the Pacific, SPK and SPC still show some eastward propagation. One hypothesis is that the transient response of the MJO to cycling between ENSO states differs from the steady-state response to a given ENSO state. For example, a decaying El Niño event may influence the oceanic and atmospheric state as the next La Niña event develops in the same year. To test this, we analyze the three 50-year SPCAM3-KPP simulations in which the ocean is constrained to the mean state of each SPC ENSO phase: SPK-EN, SPK-LN, and SPK-NN (Table 1). SPK-EN shows a strong, eastward propagating MJO (Figure 12 b), which propagates faster and further east than the MJO in all years of SPK-ENSO (Figure 12 a), but not as far east as the MJO in El Niño years of SPK-ENSO (Figure 11 c).

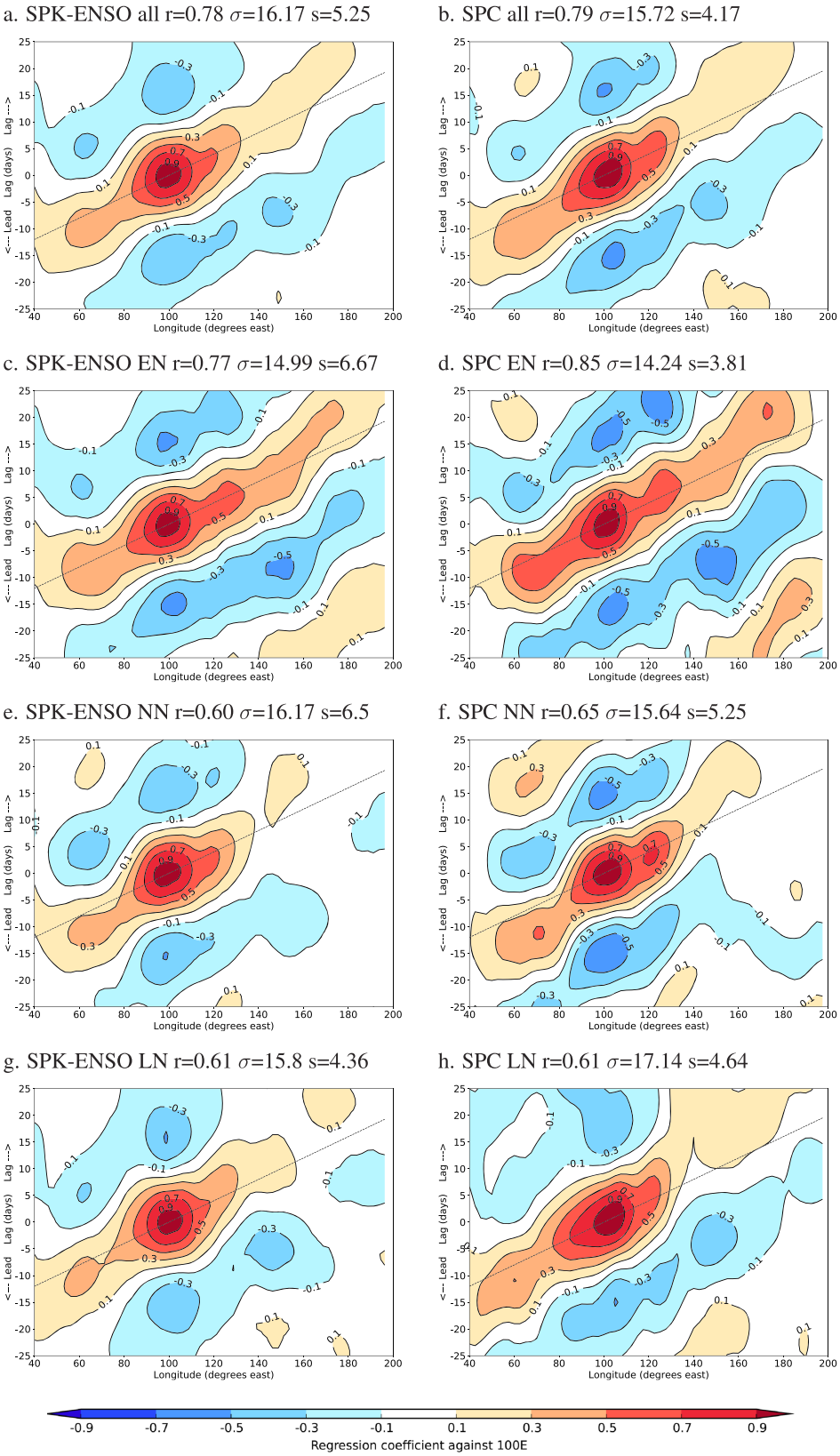

Figure 11. As in Figure 2 but for (left column) SPK-ENSO and (right column) SPC and for (a, b) all years in the simulation and (c–h) for composites by ENSO phase of (c, d) El Niño, (e, f) neutral, and (g, h) La Niña years. The SPC panels are reproduced from Figures 2 and 7 for reference.

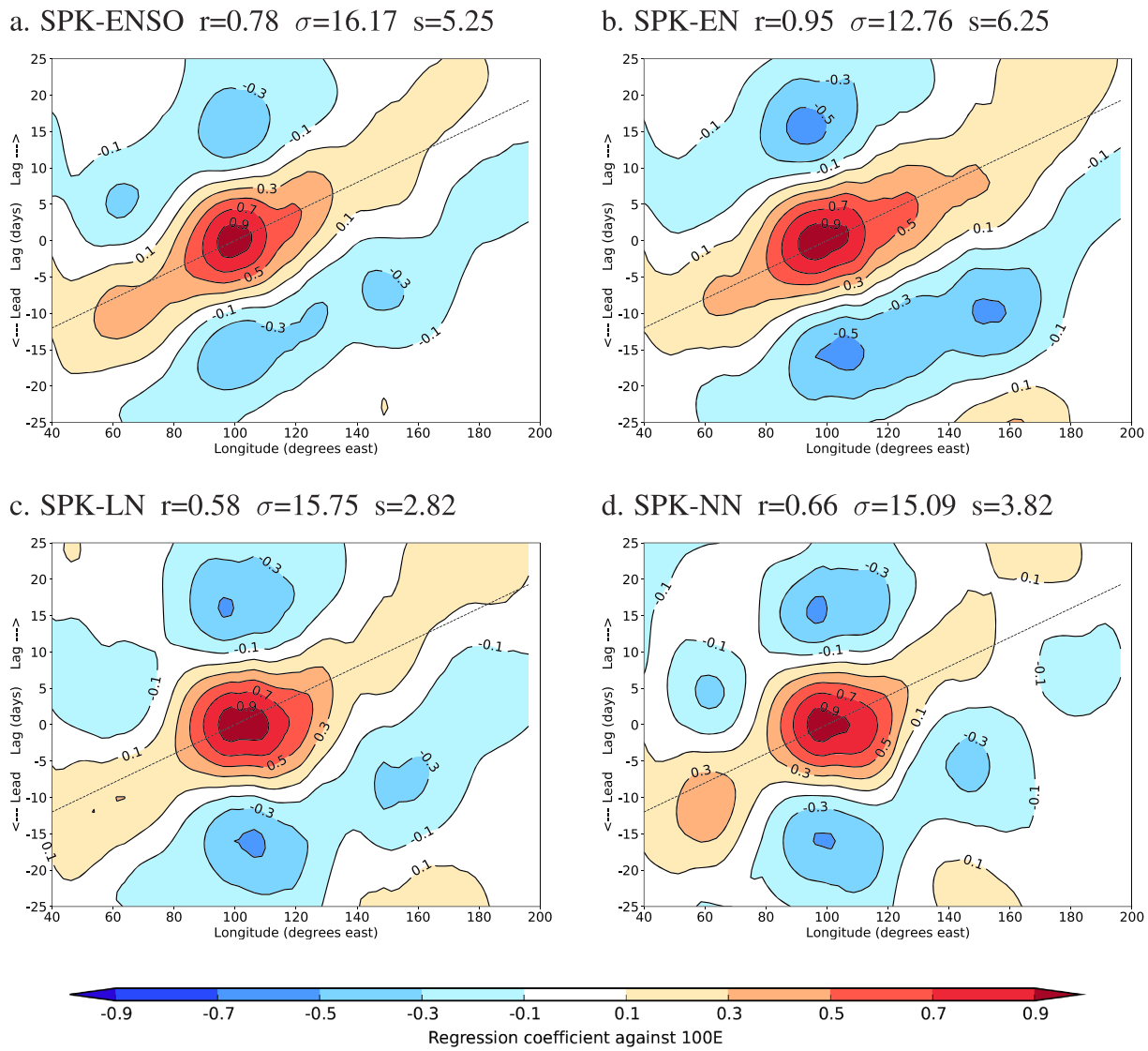

Figure 12. As in Figure 2 but for (a) SPK-ENSO, (b) SPK-EN, (c) SPK-NN, and (d) SPK-LN. The SPK-ENSO panel is reproduced from Figure 11 for reference.

SPK-NN (Figure 12 c) and SPK-LN (Figure 12 d) produce a standing oscillation near the Maritime Continent, similar to SPK-SPC. SPK-NN also shows a jump from the Indian Ocean to the Maritime Continent, similar to the neutral ENSO composite in SPK-ENSO (Figure 11 e). These results suggest that the standing oscillation in SPK-SPC arises from the steady-state response to the biases in the SPC mean ocean state. ENSO variability mitigates this response, allowing MJO propagation from the Indian Ocean to the Maritime Continent in La Niña and neutral years, potentially through lagged effects of preceding El Niño events.

These results strongly suggest that the robust MJO propagation in SPC arises from neither air-sea interactions on intraseasonal timescales, which only slightly improve MJO propagation under either the observed or SPC SST mean state or from any feature of the SPC mean state, which strongly degrades the MJO. Rather, the SPC MJO arises from the response to ENSO variability, particularly the warm Pacific SST anomalies in El Niño years that effectively cancel the SPC cold SST bias.

4. Discussion

Our results highlight that tropical systematic errors and coupled modes of interannual variability (e.g., ENSOa and IOD) can alter the perceived effects of air-sea interactions on the MJO. Many studies of air-sea feedbacks to the MJO in models have compared a CGCM to its AGCM counterpart, forced by either

observed, AMIP-type SSTs or by SSTs from the CGCM (e.g., DeMott et al., 2014, 2019; Liess et al., 2004; Rajendran & Kitoh, 2006; Zhang et al., 2006). As highlighted previously (DeMott et al., 2015; Klingaman & Woolnough, 2014a), comparing CGCM and AMIP-type AGCM simulations conflates the effects of mean state biases and air-sea feedbacks. Our study suggests that these comparisons are also flawed because they do not account for changes in interannual variability between the CGCM and AGCM, either in the phenomena themselves (e.g., CGCM biases in the representation of ENSO or the IOD) or in their teleconnections to the MJO (e.g., an overly strong MJO response to ENSO, as in SPC).

Perhaps more importantly, our results demonstrate that so-called "replay" simulations—comparisons against AGCM simulations with prescribed, interannually varying CGCM SSTs—are also problematic, because they do not cleanly isolate the effects of air-sea feedbacks within the MJO from the effects of air-sea coupling on other processes, such as the response to ENSO. For example, DeMott et al. (2014) concluded that air-sea feedbacks improved MJO propagation in SPCCSM3, based on differences between SPCCSM3 and "replay" SPCAM3 simulations with temporally smoothed SPCCSM3 SSTs. Our SPCAM3-KPP simulations reveal that the strong MJO in SPCCSM3 arises from a strong response to ENSO variability, complicated by strong mean state SST errors in the equatorial Pacific. Air-sea interactions play a secondary role, under either the SPCCSM3 or observed ocean states. We note that we did not analyze the "replay" SPCAM3 simulation with SPCCSM3 SSTs from DeMott et al. (2014). Those studies concluded that air-sea interactions improved, but were not essential to, the representation of the MJO in SPCCSM3, which supports the results here about the secondary effect of coupling. The replay SPCAM3 simulation includes the SPCCSM3 ENSO variability, but DeMott et al. (2014) did not analyze the role of coupling as a function of ENSO phase, only in the simulation as a whole. Understanding how ENSO alters air-sea interactions within the MJO, and how consequent changes in MJO structure and amplitude feed back to ENSO activity, remain active areas of future research.

Further, many CGCM-based studies of the MJO evaluate a simulation only a few decades long, perhaps 50 years at most. If the CGCM MJO responds strongly to ENSO, as it does in SPCCSM3, then the diagnosed MJO fidelity is sensitive to chaotic internal coupled variability in the CGCM. For example, one 30-year simulation of a given CGCM might contain more El Niños than La Niñas, while another might contain more La Niñas than El Niños; one simulation might exhibit excessive ENSO variance, while another shows little; one simulation might produce more central Pacific ENSO events, while another produces more eastern Pacific events. An even more important issue for model development is that a given physics perturbation, or resolution change, might systematically or randomly alter internal variability to amplify or degrade the MJO, leading to erroneous conclusions about the influence of that physical process or resolution change on the MJO. Similar issues have been recognized for climate projections, leading to the creation of large ensembles to more robustly sample natural variability (Kay et al., 2015).

These issues also affect comparisons of the role of air-sea interactions in the MJO among models, as models will differ considerably in their representations of ENSO and its teleconnections, due to differences in formulations as well as in internal variability (e.g., Bellenger et al., 2014; Langenbrunner & Neelin, 2013). We motivated our study by identifying that although MetUM and SPCCSM3 suffered from similar systematic SST errors, SPCCSM3 produced a strong MJO, while MetUM did not. We initially assumed that air-sea feedbacks to the MJO must be stronger in SPCCSM3 or that some aspect of the SPCCSM3 mean state must enhance the MJO. In light of our results, it is possible that the distinction between SPCCSM3 and MetUM lies not in simulated MJO physics, but in the response of the simulated MJO to ENSO: MetUM may have a lower ENSO variance, or the response of the background state to El Niño may favor MJO propagation in SPCCSM3 more than in MetUM. Given the same ENSO variability as SPCCSM3, MetUM might produce a strong MJO. These results particularly affect the conclusions of CGCM-AGCM intercomparison studies, where the CGCM includes a dynamical ocean capable of simulating ENSO (e.g., DeMott et al., 2019; Rajendran & Kitoh, 2006; Zhang et al., 2006). Relatedly, we note that our analysis based on only one GCM, which produces a strong MJO, excessive intraseasonal variance in rainfall, and high ENSO variance, and which uses an unconventional treatment of convection. We anticipate further studies with other GCMs in a similar atmosphere-ocean-mixed-layer coupled framework, to confirm these results.

The interpretation of our simulations is complicated by slight variations in the basic state between experiments. SPK-SPC and SPK-ENSO are systematically drier near the Maritime Continent relative to SPC (Figure 10), associated with a slight cold SST bias (Figure 8). These differences may be sufficient to reduce

the zonal moisture gradient across the Indian Ocean and inhibit propagation across the Maritime Continent (e.g., Gonzalez & Jiang, 2017; Kim et al., 2017). We cannot rule out the influence of these errors on the poor MJO propagation in SPK-SPC relative to SPC or the slightly weaker MJO propagation in SPK-ENSO relative to SPC. However, we note that SPK-ENSO produces a strong MJO in spite of these biases; comparing SPK-SPC and SPK-ENSO, both affected by these biases, clearly shows that include the SPC ENSO cycle dramatically improves the MJO.

We recommend that future model studies of air-sea interactions in the MJO control for the effects on the background state of not only model systematic errors but also interannual variability. The atmosphere-ocean-mixed-layer framework presented here is an effective way to control for these factors, but other methods include restoring the ocean state to an observed climatology with flux corrections—with a relaxation timescale suitably long so as not to damp ISV—or subsampling only a certain phase of variability (e.g., ENSO neutral) in a simulation. Isolating the role of air-sea interactions on intraseasonal scales remains challenging, but the systematic isolation of mean state biases and interannual variability presented here shows a path to more tightly constraining the problem.

5. Conclusions

The MJO is often poorly simulated in climate models, which limits our understanding of its basic physics and creates uncertainty in regional projections of climate change, since the MJO is a major cause of extreme weather globally. Including air-sea interactions in models frequently improves the MJO (DeMott et al., 2015, and references therein), but the aspects of the MJO that improve (e.g., propagation speed, amplitude, and period) and the degree of improvement vary among models. It remains unclear whether air-sea feedbacks are important to the real-world MJO, in part because model sensitivity experiments have not identified a consistent mechanism by which air-sea coupled processes influence intraseasonal tropical convection. Model intercomparison efforts are hampered by intermodel variability in the simulated basic state, elements of which influence MJO propagation (e.g., Crueger et al., 2013; Inness & Slingo, 2003; Klingaman & Woolnough, 2014b).

SPCCSM3 produces one of the best representations of the MJO among contemporary models (Jiang et al., 2015), including relative to its counterpart atmosphere-only model, SPCAM3 (e.g., DeMott et al., 2014; Stan et al., 2010). However, SPCCSM3 exhibits similar systematic errors to other coupled models, including MetUM, in which those biases strongly degraded the MJO (Klingaman & Woolnough, 2014b). Previous studies with SPCCSM3 assessed the role of air-sea interactions under only this biased mean state, and did not consider the effects of interannual variability (e.g., ENSO) on the background state for the MJO.

To more thoroughly investigate the mechanisms underlying the realistic representation of the MJO in SPCCSM3, we systematically isolated the effects of (a) intraseasonal air-sea coupled feedbacks, (b) mean state SST errors, and (c) ENSO on the simulated MJO. We accomplished this through a new model configuration, SPCAM3-KPP, in which SPCAM3 is coupled to many columns of a one-dimensional ocean model, similar to Hirons et al. (2015) for MetUM. SPCAM3-KPP can be easily constrained to a target state, which in this study includes the observed mean annual cycle, the SPCCSM3 mean annual cycle, and a repeating 3-year composite ENSO cycle from SPCCSM3. The lack of a direct simulation of ENSO and IOD in SPCAM3-KPP limits the potentially complicating effects of these modes on our analysis of the MJO.

Under the observed ocean mean state, SPCAM3-KPP produces a coherent, eastward propagating MJO. A "replay" SPCAM3 simulation—with prescribed, interannually varying SSTs from SPCAM3-KPP—shows a slightly weaker, but still strong MJO, suggesting that intraseasonal air-sea feedbacks are not essential to MJO propagation in SPCAM3-KPP under the observed ocean mean state. Under the SPCCSM3 ocean mean state, SPCAM3-KPP fails to produce an MJO, in stark contrast to SPCCSM3 itself. Again, air-sea feedbacks make little difference to simulated ISV. When the SPCCSM3 ENSO cycle is imposed, on top of the SPCCSM3 ocean mean state, SPCAM3-KPP generates an MJO highly similar to that in SPCCSM3, suggesting high ENSO variance is associated with the strong SPCCSM3 MJO, in spite of its systematic errors. Further analysis shows that SPCCSM3, and SPCAM3-KPP with the imposed SPCCM3 ENSO cycle, displays a strong MJO only in El Niño years, when anomalously warm equatorial Pacific SSTs counteract the cold systematic SST biases. In neutral and La Niña years, SPCCSM3 produces little MJO activity, in contrast to observations.

The potential for strong ENSO feedbacks to the MJO complicates the evaluation of the MJO in models generally and the identification of air-sea interactions in the MJO specifically. Most model evaluations and intercomparisons are performed with only a few decades of simulation at most, leaving them highly sensitive to the effects of chaotic internal variability that could alter ENSO statistics and ENSO-MJO teleconnections through changes to the basic state. Future modeling efforts that aim to isolate the role of air-sea interactions in the MJO in climate models should control for the influence of interannual variability, as well as for coupled-model systematic errors.

Acknowledgments
The AMIP sea ice data set can be obtained from the https://pcmdi.llnl.gov/mips/amip website. The NOAA OI SST data set can be obtained from the website (https://www.esrl.noaa.gov/psd/data/gridded/data.noaa.oisst.v2.highres.html). NOAA OLR data can be obtained from the website (https://www.esrl.noaa.gov/psd/data/gridded/data.interp_OLR.html). ERA-Interim reanalyses can be obtained from the https://www.ecmwf.int/en/forecasts/datasets/reanalysis-datasets/era-interim website. The Smith and Murphey (2007) ocean analyses and data from all simulations analyzed are stored on the JASMIN collaborative analysis facility (http://jasmin.ac.uk). Access to data can be obtained by contacting Nicholas Klingaman (nicholas.klingaman@ncas.ac.uk). Nicholas Klingaman was funded by an Independent Research Fellowship from the Natural Environment Research Council (NE/L010976/1) and a grant from the NOAA Modeling, Analysis, Predictions and Projections program (NA16OAR4310071). Charlotte DeMott was funded by the National Science Foundation (NSF 1445191) and the National Oceanic and Atmospheric Administration Modeling, Analysis, Predictions and Projections program (NOAA MAPP NA16OAR4310094). SPCAM-KPP simulations were performed on ARCHER, the U.K. national supercomputing facility (http://www.archer.ac.uk). The authors are grateful for productive discussions with Steve Woolnough and other members of the MJO Task Force.

References

Ahn, M.-S., Kim, D., Sperber, K. R., Kang, I.-S., Maloney, E., Waliser, D., & Hendon, H. (2017). Mjo simulation in CMIP5 climate models: MJO skill metrics and process-oriented diagnosis. *Climate Dynamics*, *49*, 4023–4045.

Bellenger, H., Guilyardi, E., Leloup, J., Lengaigne, M., & Vialard, J. (2014). ENSO representation in climate models: From CMIP3 to CMIP5. *Climate Dynamics*, *42*, 1999–2018.

Benedict, J. J., & Maloney, E. D. (2013). Tropical intraseasonal variability in version 3 of the GFDL atmosphere model. *Journal of Climate*, *26*, 426–449.

Benedict, J. J., & Randall, D. A. (2009). Structure of the Madden–Julian oscillation in the superparameterized CAM. *Journal of Climate*, *66*, 3277–3296.

Benedict, J. J., & Randall, D. A. (2011). Impacts of idealized air–sea coupling on Madden–Julian oscillation structure in the superparameterized CAM. *Journal of the Atmospheric Sciences*, *68*, 1990–2008.

Bernie, D. J., Guilyardi, E., Madec, G., Slingo, J. M., Woolnough, S. J., & Cole, J. (2008). Impact of resolving the diurnal cycle in an ocean–atmosphere GCM. Part 2: A diurnally coupled CGCM. *Climate Dynamics*, *31*, 909–925.

Bernie, D. J., Woolnough, S. J., & Slingo, J. M. (2005). Modeling diurnal and intraseasonal variability of the ocean mixed layer. *Journal of Climate*, *18*, 1190–1202.

Camargo, S. J., Robertson, A. W., Barnston, A. G., & Ghil, M. (2008). Clustering of eastern North Pacific tropical cyclone tracks: ENSO and MJO effects. *Geochemistry, Geophysics, Geosystems*, *9*, Q06V05. https://doi.org/10.1029/2007gc001861

Cassou, C. (2008). Intraseasonal interaction between the Madden–Julian oscillation and the North Atlantic oscillation. *Nature*, *455*, 523–527.

Crueger, T., Stevens, B., & Brokopf, R. (2013). The Madden-Julian oscillation in ECHAM6 and the introduction of an objective MJO metric. *Journal of Climate*, *26*, 3241–3257.

Danbasoglu, G., Large, W. G., Tribbia, J. J., Gent, P. R., Briegleb, B. P., & McWilliams, J. (2006). Diurnal coupling in the tropical oceans of CCSM3. *Journal of Climate*, *19*, 2347–2365.

DeMott, C. A., Benedict, J. J., Klingaman, N. P., Woolnough, S. J., & Randall, D. A. (2016). Diagnosing ocean feedbacks to the MJO: SST-modulated surface fluxes and the moist static energy budget. *Journal of Geophysical Research: Atmopheres*, *121*, 8350–8373. https://doi.org/10.1002/2016JD025098

DeMott, C. A., Klingaman, N. P., Tseng, W.-L., Burt, M. A., Gao, Y., & Randall, D. A. (2019). The convection connection: How ocean feedbacks affect tropical mean moisture and MJO propagation. *Journal of Geophysical Research*. in review

DeMott, C. A., Klingaman, N. P., & Woolnough, S. J. (2015). Atmosphere–ocean coupled processes in the Madden–Julian oscillation. *Reviews of Geophysics*, *53*, 1099–1154. https://doi.org/10.1002/2014RG000478

DeMott, C. A., Randall, D. A., & Khairoutdinov, M. (2007). Convective precipitation variability as a tool for general circulation model analysis. *Journal of Climate*, *20*, 91–112.

DeMott, C. A., Stan, C., Randall, D. A., & Branson, M. D. (2014). Intraseasonal variability in Coupled GCMs: The roles of ocean feedbacks and model physics. *Journal of Climate*, *27*(13), 4970–4995. https://doi.org/10.1175/jcli-d-13-00760.1

Demott, C. A., Wolding, B. O., Maloney, E. D., & Randall, D. A. (2018). Atmospheric mechanisms for MJO decay over the Maritime Continent. *Journal of Geophysical Research: Atmopheres*, *123*, 5188–5204. https://doi.org/10.1029/2017JD026979

Gonzalez, A. O., & Jiang, X. (2017). Winter mean lower tropospheric moisture over the Maritime Continent as a climate model diagnostic metric for the propagation of the Madden–Julian oscillation. *Geophysical Research Letters*, *44*, 2588–2596. https://doi.org/10.1002/2016GL072430

Gushchina, D., & Dewitte, B. (2012). Intraseasonal tropical atmospheric variability associated with the two flavors of El Niño. *Monthly Weather Review*, *140*, 3669–3681.

Halkides, D. J., Waliser, D. E., Lee, T., Menemenlis, D., & Guan, B. (2015). Quantifying the processing controlling intraseasonal mixed-layer temperature variability in the tropical Indian Ocean. *Journal of Geophysical Research: Oceans*, *120*, 692–715. https://doi.org/10.1002/2014JC010139

Hannah, W. M., & Maloney, E. D. (2011). The role of moisture–convection feedbacks in simulating the Madden–Julian oscillation. *Journal of Climate*, *24*, 2754–2770.

Hendon, H. H., Zhang, C., & Glick, J. D. (1999). Interannual variation of the Madden–Julian oscillation during austral summer. *Journal of Climate*, *12*, 2538–2550.

Hirons, L. C., Inness, P., Vitart, F., & Bechtold, P. (2013). Understanding advances in the simulation of intraseasonal variability in the ECMWF model. Part I: The representation of the MJO. *Quarterly Journal of the Royal Meteorological Society*, *139*, 1427–1444. https://doi.org/10.1002/qj.2060

Hirons, L. C., Klingaman, N. P., & Woolnough, S. J. (2015). MetUM-GOML: A near-globally coupled atmosphere–ocean-mixed-layer model. *Geoscientific Model Development*, *8*, 363–379.

Hirons, L. C., Klingaman, N. P., & Woolnough, S. J. (2018). The impact of air–sea interactions on the representation of tropical precipitation extremes. *Journal of Advances in Modeling Earth Systems*, *10*, 550–559. https://doi.org/10.1002/2017MS001252

Holloway, C. E., Woolnough, S. J., & Lister, G. M. S. (2013). The effects of explicit versus parameterized convection on the MJO in a large-domain high-resolution tropical case study. Part I: Characterization of large-scale organization and propagation. *Journal of the Atmospheric Sciences*, *70*, 1342–1369.

Hung, M.-P., Lin, J.-L., Wang, W., Kim, D., Shinoda, T., & Weaver, S. J. (2013). MJO and convectively coupled equatorial waves simulated by CMIP5 climate models. *Journal of Climate*, *26*(17), 6185–6214. https://doi.org/10.1175/jcli-d-12-00541.1

Hurrell, J. W., Hack, J. J., Shea, D., Caron, J. M., & Rosinski, J. (2008). A new sea surface temperature and sea ice boundary data set for the Community Atmospheric Model. *Journal of Climate*, *21*, 5145–5153.

Inness, P. M., & Slingo, J. M. (2003). Simulation of the Madden–Julian oscillation in a coupled general circulation model. Part I: Comparison with observations and an atmosphere-only GCM. *Journal of Climate*, *16*, 345–364.

Inness, P. M., Slingo, J. M., Guilyardi, E., & Cole, J. (2003). Simulation of the Madden–Julian oscillation in a coupled general circulation model. Part II: The role of the basic state. *Journal of Climate*, *17*, 365–382.

Jiang, X., Waliser, D. E., Xavier, P. K., Petch, J., Klingaman, N. P., Woolnough, S. J., et al. (2015). Vertical structure and physical processes of the Madden–Julian oscillation: Exploring key model physics in climate simulations. *Journal of Geophysical Research: Atmospheres*, *120*, 4718–4748. https://doi.org/10.1002/2014JD022375

Johnson, R. H., Ciesielski, P. E., & Ruppert, J. H. Jr. (2015). Sounding-based thermodynamic budgets for DYNAMO. *Journal of the Atmospheric Sciences*, *72*, 598–622.

Jones, C., Carvalho, L. M. V., Higgins, R. W., Waliser, D. E., & Schemm, J.-K. E. (2004). Climatology of tropical intraseasonal convective anomalies: 1979–2002. *Journal of Climate*, *17*, , 523–539.

Kay, J. E., Deser, C., Phillips, A., Mai, A., Hannay, C., Strand, G., et al. (2015). The Community Earth System Model (CESM) Large Ensemble project: A community resource for studying climate change in the presence of internal climate variability. *Bulletin of the American Meteorological Society*, *96*, 1333–1349.

Khairoutdinov, M., Randall, D., & DeMott, C. (2005). Simulations of the atmospheric general circulation using a cloud-resolving model as a superparameterization of physical processes. *Journal of the Atmospheric Sciences*, *62*, 2136–2154. https://doi.org/10.1175/jas3453.1

Khairoutdinov, M. F., DeMott, C. A., & Randall, D. A. (2008). Evaluation of the simulated interannual and subseasonal variability in an AMIP-style simulation using the CSU Multiscale Modeling Framework. *Journal of Climate*, *21*, 413–431.

Kim, D., Kim, H., & Lee, M.-I. (2017). Why does the MJO detour the Maritime Continent during austral summer? *Geophysical Research Letters*, *44*, 2579–2587. https://doi.org/10.1002/2017GL072643

Kim, D., Sobel, A. H., Frierson, D. M. W., Maloney, E. D., & Kang, I.-S. (2011). A systematic relationship between intraseasonal variability and mean state bias in AGCM simulations. *Journal of Climate*, *24*, 5506–5520.

Klingaman, N. P., Jiang, X., Xavier, P. K., Petch, J., Waliser, D., & Woolnough, S. J. (2015). Vertical structure and physical processes of the Madden–Julian oscillation: Synthesis and summary. *Journal of Geophysical Research: Atmospheres*, *120*, 4671–4689. https://doi.org/10.1002/2015JD023196

Klingaman, N. P., & Woolnough, S. J. (2014a). Using a case-study approach to improve the Madden–Julian oscillation in the Hadley Centre model. *Quarterly Journal of the Royal Meteorological Society*, *140*, 2491–2505.

Klingaman, N. P., & Woolnough, S. J. (2014b). The role of air–sea coupling in the simulation of the Madden–Julian oscillation in the Hadley Centre model. *Quarterly Journal of the Royal Meteorological Society*, *140*, 2272–2286.

Klingaman, N. P., Woolnough, S. J., Weller, H., & Slingo, J. M. (2011). The impact of finer-resolution air-sea coupling on the intraseasonal oscillation of the Indian summer monsoon. *Journal of Climate*, *24*, 2451–2468.

Langenbrunner, B., & Neelin, J. D. (2013). Analyzing ENSO teleconnection in CMIP models as a measure of model fidelity in simulating precipitation. *Journal of Climate*, *26*, 4431–4446.

Large, W., McWilliams, J., & Doney, S. (1994). Oceanic vertical mixing: A review and a model with a nonlocal boundary layer parameterization. *Reviews of Geophysics*, *32*, 363–403.

Lau, K.-M., & Sui, C.-H. (1997). Mechanisms of short-term sea surface temperature regulation: observations during TOGA COARE. *Journal of Climate*, *10*, 465–472.

Lawrence, D. M., & Webster, P. J. (2002). The boreal intraseasonal oscillation: Relationship between northward and eastward movement of convection. *Journal of the Atmospheric Sciences*, *59*, 1593–1606.

Liess, S., Bengtsson, L., & Arpe, K. (2004). The intraseasonal oscillation in ECHAM4. Part I: Coupled to a comprehensive ocean model. *Climate Dynamics*, *22*, 671–688.

Lin, H., Brunet, G., & Derome, J. (2009). An observed connection between the North Atlantic Oscillation and the Madden–Julian oscillation. *Journal of Climate*, *22*, 364–380.

Lin, J.-L., Weickman, K. M., Kiladis, G. N., Mapes, B. E., Schubert, S. D., Suarez, M. J., et al. (2008). Subseasonal variability associated with Asian summer monsoon simulated by 14 IPCC AR4 coupled GCMs. *Journal of Climate*, *21*, 4542–4566.

Lorenz, D. J., & Hartmann, D. L. (2006). The effect of the MJO on the North American monsoon. *Journal of Climate*, *19*, 333–343. https://doi.org/10.1175/jcli3684.1

Madden, R. A., & Julian, P. R. (1971). Detection of a 40–50 day oscillation in the zonal wind in the tropical Pacific. *Journal of the Atmospheric Sciences*, *28*, 702–708.

Madden, R. A., & Julian, P. R. (1972). Description of global-scale circulation cells in the tropics with a 40–50 day period. *Journal of the Atmospheric Sciences*, *29*, 1109–1123.

Maloney, E. D., & Hartmann, D. L. (2000). Modulation of eastern North Pacific hurricanes by the Madden–Julian oscillation. *Journal of Climate*, *13*, 1451–1460.

Miyakawa, T., Satoh, M., Miura, H., Tomita, H., Yashiro, H., Noda, A. T., et al. (2014). Madden–Julian oscillation prediction skill of a new-generation global model demonstrated using a supercomputer. *Nature Communications*, *5*, 3769.

Peatman, S. C., & Klingaman, N. P. (2018). The Indian summer monsoon in MetUM-GOML2: Effects of coupling and resolution. *Geoscientific Model Development*, *11*, 4693–4709.

Pegion, K., & Kirtman, B.-P. (2008). The impact of air–sea interactions on the predictability of the tropical intraseasonal oscillation. *Journal of Climate*, *21*, 5870–5886.

Pohl, B., & Matthews, A. J. (2007). Observed changes in the lifetime and amplitude of the Madden–Julian oscillation associated with interannual ENSO sea surface temperature anomalies. *Journal of Climate*, *20*, 2659–2674.

Rajendran, K., & Kitoh, A. (2006). Modulation of tropical intraseasonal oscillations by atmosphere-ocean coupling. *Journal of Climate*, *19*, 366–391.

Reynolds, R., Rayner, N., Smith, T. M., Stokes, D. C., & Wang, W. (2002). An improved in situ and satellite SST analysis for climate. *Journal of Climate*, *15*, 1609–1625.

Seo, K.-H., Schemm, J.-K. E., Wang, W., & Kumar, A. (2007). The boreal summer intraseasonal oscillation simulations in the NCEP Climate Forecast System: The effect of sea surface temperature. *Monthly Weather Review*, *135*, 1807–1827.

Slingo, J. M., Sperber, K. R., Boyle, J. S., Ceron, J. P., Dix, M., Dugas, B., et al. (1996). Intraseasonal oscillations in 15 atmospheric general circulation models: Results from an AMIP diagnostic subproject. *Climate Dynamics*, *12*(5), 325–357.

Smith, D. M., & Murphey, J. M. (2007). An objective ocean temperature and salinity analysis using covariances from global climate models. *Journal of Geophysical Research*, *112*, C02022. https://doi.org/10.1029/2005JC003172

Smith, R., and P. Gent (2004), Reference manual for the Parallel Ocean Program ocean component of the Community Climate System Model (CCSM2.0 and 3.0), *LANL/NCAR Technical report LAUR-02-2484*.
Sperber, K. R. (2004). Madden–Julian variability in NCAR CAM2.0 and CCSM2.0. *Climate Dynamics*, *23*, 259–278.
Sperber, K. R., Gualdi, S., Legutke, S., & Gayler, V. (2005). The Madden–Julian oscillation in ECHAM4 coupled and uncoupled general circulation models. *Climate Dynamics*, *25*, 117–140.
Stan, C., Khairoutdinov, M., DeMott, C. A., Krishnamurthy, V., Straus, D. M., Randall, D. A., et al. (2010). An ocean-atmosphere climate simulation with an embedded cloud resolving model. *Geophysical Research Letters*, *37*, L01702. https://doi.org/10.1029/2009gl040822
Tam, C.-Y., & Lau, N.-C. (2005). Modulation of the Madden–Julian oscillation by ENSO: Inferences from observations and GCM simulations. *Journal of the Meteorological Society of Japan*, *83*, 727–743.
Taylor, K. E., Stouffer, R. J., & Meehl, G. A. (2012). An overview of CMIP5 and the experiment design. *Bulletin of the American Meteorological Society*, *93*, 485–498.
Tseng, W.-L., Tsuang, B.-J., Keenlyside, N. S., Hsu, H.-H., & Tu, C.-Y. (2015). Resolving the upper–ocean warm layer improves the simulation of the Madden–Julian oscillation. *Climate Dynamics*, *44*, 1487–1503.
Vitart, F. (2009). Impact of the Madden Julian oscillation on tropical storms and risk of landfall in the ECMWF forecast system. *Geophysical Research Letters*, *36*, L15802. https://doi.org/10.1029/2009GL039089
Vitart, F., & Molteni, F. (2010). Simulation of the Madden–Julian oscillation and its teleconnections in the ECMWF forecast system. *Quarterly Journal of the Royal Meteorological Society*, *136*, 842–855.
Wang, L., Li, T., Maloney, E., & Wang, B. (2017). Fundamental causes of propagating and nonpropagating MJOs in MJOTF/GASS models. *Journal of Climate*, *30*, 3743–3769.
Webber, B. G. M., Matthews, A. J., & Heywood, K. J. (2010). A dynamical ocean feedback mechanism for the Madden–Julian oscillation. *Quarterly Journal of the Royal Meteorological Society*, *136*, 740–754.
Webber, B. G. M., Matthews, A. J., Heywood, K. J., & Stevens, D. P. (2012). Ocean Rossby waves as a triggering mechanism for primary Madden–Julian events. *Quarterly Journal of the Royal Meteorological Society*, *138*, 514–527.
Wheeler, M. C., Hendon, H. H., Cleland, S., Meinke, H., & Donald, A. (2009). Impacts of the Madden–Julian oscillation on Australian rainfall and circulation. *Journal of Climate*, *22*, 1482–1498.
Wilson, E. A., Gordon, A. L., & Kim, D. (2013). Observations of the Madden Julian oscillation during Indian Ocean dipole events. *Journal of Geophysical Research*, *118*, 2588–2599. https://doi.org/10.1002/jgrd.50241
Woolnough, S. J., Slingo, J. M., & Hoskins, B. J. (2000). The relationship between convection and sea surface temperatures on intraseasonal timescales. *Journal of Climate*, *13*(12), 2086–2104.
Zhang, C. (2005). Madden–Julian oscillation. *Reviews of Geophysics*, *43*, RG2003. https://doi.org/10.1029/2004RG000,158
Zhang, C., Dong, M., Gualdi, S., Hendon, H. H., Maloney, E. D., Marshall, A., et al. (2006). Simulations of the Madden–Julian oscillation in four pairs of coupled and uncoupled global models. *Climate Dynamics*, *27*, 573–592.